Modeling for Simulation of Fluidized-Bed Incineration Process

F. Marias
Laboratoire de Génie des Procédés de Pau (EA 1932), ENSGTI, 64000 Pau, France

J. R. Puiggali
Laboratoire Energétique et Phènomènes de Transfert (UMR CNRS 8508), 33405 Talence Cedex, France

G. Flamant
Institut de Science et de Génie des Matériaux et Procédés, CNRS-IMP, 66125 Font Romeu, France

A mathematical model for the fluidized-bed incineration process was developed using the waste composed of wood, cardboard and polyvinyl chloride. It is based on heat and mass balances of the gas held within the five zones representing both the bubbling bed and freeboard and including heat transfer with sand and reacting particles of char (pyrolysis residue). The mixture fraction concept and assumption of chemical equilibrium are used to compute temperature and species concentration fields resulting from volatile combustion. These fields are affected by char combustion, which relies, in turn, on a model based on surface reaction and a full population balance. The formation of pollutants (NO_x, SO_x) was also taken into account. The main steps involved by the numerical resolution of the model are discussed, and some results are shown for a 1 MW unit.

Introduction

This study is a part of a global project devoted to the construction of a real-time incineration simulator. Such a simulator might be used as a learning tool for process operators. To be effective, this learning tool must take into account as many physical phenomena as possible. Because of the wide variety of technologies used to reduce the mass and volume of waste, the simulator must include several submodels to describe these technologies. For instance, several models of furnace behavior (rotary kiln, grating furnace, and fluidized bed) in addition to models for dust removal and gas cleaning (such as an electrostatic precipitator or scrubbing towers) are necessary.

The first attempt is to develop a model for a fluidized-bed incineration process. In the case of coal combustion (Avedesian and Davidson, 1973; Gordon and Admundson, 1976; Lee et al., 1980; Park et al., 1980; Stannmore and Jung, 1980; Ross et al., 1981; Turnbull and Kossakowski, 1984; El Mezni, 1985; La Nauze, 1985; Agarwal and Wildegger-Gaissmaier, 1987; Preto, 1987; Prins, 1987; De Souza-Santos, 1989; Brem, 1990; Stubington and Chan, 1990; Wildegger-Gaismaier and Agarwal, 1990; Adanez and Abanades, 1992a,b; Junk and Brown, 1993; Hannes, 1996; Sriramulu et al., 1996), such a technology provides many advantages such as temperature homogenization, intensive heat and mass transfer, and high thermal capacity allowing for variations in supply composition and flow rate. These advantages suggest the choice of a fluidized-bed process for incineration (Paladino et al., 1992; Ogada and Werther, 1996).

Because of the wide variations in municipal waste (Ademe, 1998), the characterization of the fuel entering the boiler is not obvious. In order to reduce the modeling effort, only representative components of waste are used, namely, wood, cardboard, and polyvinyl chloride. Following the work of several researchers (Beck and Wang, 1980; Shafizadeh, 1982; El Ghezal, 1983; Graham and Bergougnou, 1984; Hemati, 1984; Dif, 1987; Bilodeau et al., 1993), flash pyrolysis is expected to occur in a hot fluidized bed. In assuming this method of operation, an equivalent input, convenient for our modeling purposes is built.

Correspondence concerning this article should be addressed to F. Marias.

As in fluidized combustion of coal, the major difficulty in the modeling effort arises from the description of the hydrodynamic behavior of the bubbling bed. Literature provides many models (Davidson and Harrison, 1963; Kato and Wen, 1969; Bukur and Amundson, 1975; Werther, 1980; Kunii and Levenspiel, 1991) which may be classified, in order of complexity, from a pseudo-homogeneous phase model to complex three phase or bubble assemblage models. A modified Werther's (1980) model has been chosen. This modified model replaces Werther's film by a two-dimensional reactive zone. Finally, the freeboard region of the bed is summed up as two perfectly stirred zones describing disengaging height and the post combustion zone.

Balance equations for gaseous components, as well as a population balance for char, are proposed in this article. Moreover, the pollutant formation route is included to provide NO_x and SO_x concentration. Several typical results of the model for steady-state operation are presented in the final part of the article.

From Ordinary Waste to Process Input

In France, as indicated by Ademe (1998), municipal waste is mainly composed of wood, glass, metals, plastics, textiles, leather, paper, and cardboard. Not all of these materials are directly concerned with incineration. For example, iron and steel are removed by magnetic separators. Moreover, only relevant components of the remaining waste are of interest for modeling purposes. Consequently, the municipal waste used, as an input for the fluidized-bed incineration process, is composed of wood, cardboard, and plastics. This composition is not sufficient to describe the physico-chemical steps occurring in such an incinerator. First of all, proximate and ultimate analysis are required. Secondly, assuming flash pyrolysis is to occur in hot fluidized beds (Beck and Wang, 1980; Shafizadeh, 1982; El Ghezal, 1983; Graham and Bergougnou, 1984; Hemati, 1984; Dif, 1987; Bilodeau et al., 1993), data relative to this phenomenon and applied to our waste is required.

Waste is assumed to be shredded before it is fed to the furnace. Particles issued from shredding are assumed to be spherical, and their size distribution to be ϕ_0.

Chemical waste characterization

Ordinary waste is composed of a wide variety of wood, cardboard, and plastics with different moisture content. In this study, regular materials are considered and the moisture content is set to an intermediate value. From El Ghezal (1983), Robert (1989), and Zhou (1994), composition of wood and cardboard has been studied, allowing the formation of average materials such as those depicted in Table 1. Polyvinyl chloride is assumed to be relevant as a plastic waste because of its high chlorine content. Its ultimate and proximate analysis are given in Table 1.

Table 1. Proximate and Ultimate Analysis of Ordinary Waste

	Wood	Cardboard	P.V.C.
Proximate analysis (wt. %)			
Moisture (raw)	15.00	15.00	0.00
Fixed Carbon (db)	18.00	12.94	0.00
Volatiles (db)	81.00	81.72	100.00
Ash (db)	1.00	5.34	0.00
Lower heating value ($MJ \cdot kg^{-1} \cdot db$)	18.2	15.6	19.0
Ultimate analysis (wt. % db)			
C	50.90	43.73	38.40
H	5.76	5.70	4.80
O	42.10	44.93	0.00
N	0.20	0.09	0.00
S	0.04	0.21	0.00
Cl	0.00	0.00	56.80

Flash pyrolysis of ordinary waste

The occurrence of flash pyrolysis leads to the concept of equivalent waste. This concept involves: instantaneous drying and pyrolysis as the waste is fed to the bed; total gasification of the volatile content; pyrolysis residue composed of fixed carbon and ashes; the pyrolysis residue size distribution is equal to that of the initial waste; and gasification of nitrogen and sulfur content at atomic state.

Chemical species which compose volatile matter, as well as heat required by pyrolysis enthalpy, are taken from the literature (Baker, 1975; Beck and Wang, 1980; Deglise and Lede, 1980; Caubet et al., 1982; Shafizadeh, 1982; Delburgo and Mellotée, 1983; El Ghezal, 1983; Graham and Bergougnou, 1984; Hemati, 1984; Dif, 1987; Robert, 1989; Kashiwagi and Nambu, 1992; Bockhorn et al., 1996; Vovelle and Delfau, 1997).

As shown in Figure 1, for the case of wood, the computation of the equivalent waste is performed in three steps. The first one (endothermic instantaneous drying) preserves the size distribution of the material. It is assumed that drying only affects the internal structure, and results in a decrease in material density. In the second step, the flash pyrolysis of wood is expected, when energy is supplied. The material breaks into two components: a gaseous one composed of volatile, nitrogen, and sulfur at atomic state, and a solid one composed of fixed carbon and ashes. Once again, it is assumed that the size distribution of solid material stays constant. The last step allows us to compute the composition of the volatile matter through a balance on atomic elements and balance on energy released by the combustion of the initial material and the equivalent material (Marias, 1999).

Applying this scheme to the two other materials of the model waste, one is able to compute the equivalent waste for any given composition of the model waste. As a representation, Figure 2 shows the composition of the equivalent waste in terms of volatile, fixed carbon and pollutants vs. the initial waste. Ternary diagrams have been used to represent these dependences because of the 3-D nature of the modeled rubbish. Such a representation is used in Figure 3 to show the evolution of the volatile matter in terms of the molar fraction of relevant compounds.

Mathematical Modeling

Several studies have been published about the modeling of combustion of coal in a fluidized bed (as quoted in the introduction). Because incineration is indeed combustion, one can try to use such models in this particular case. Nevertheless,

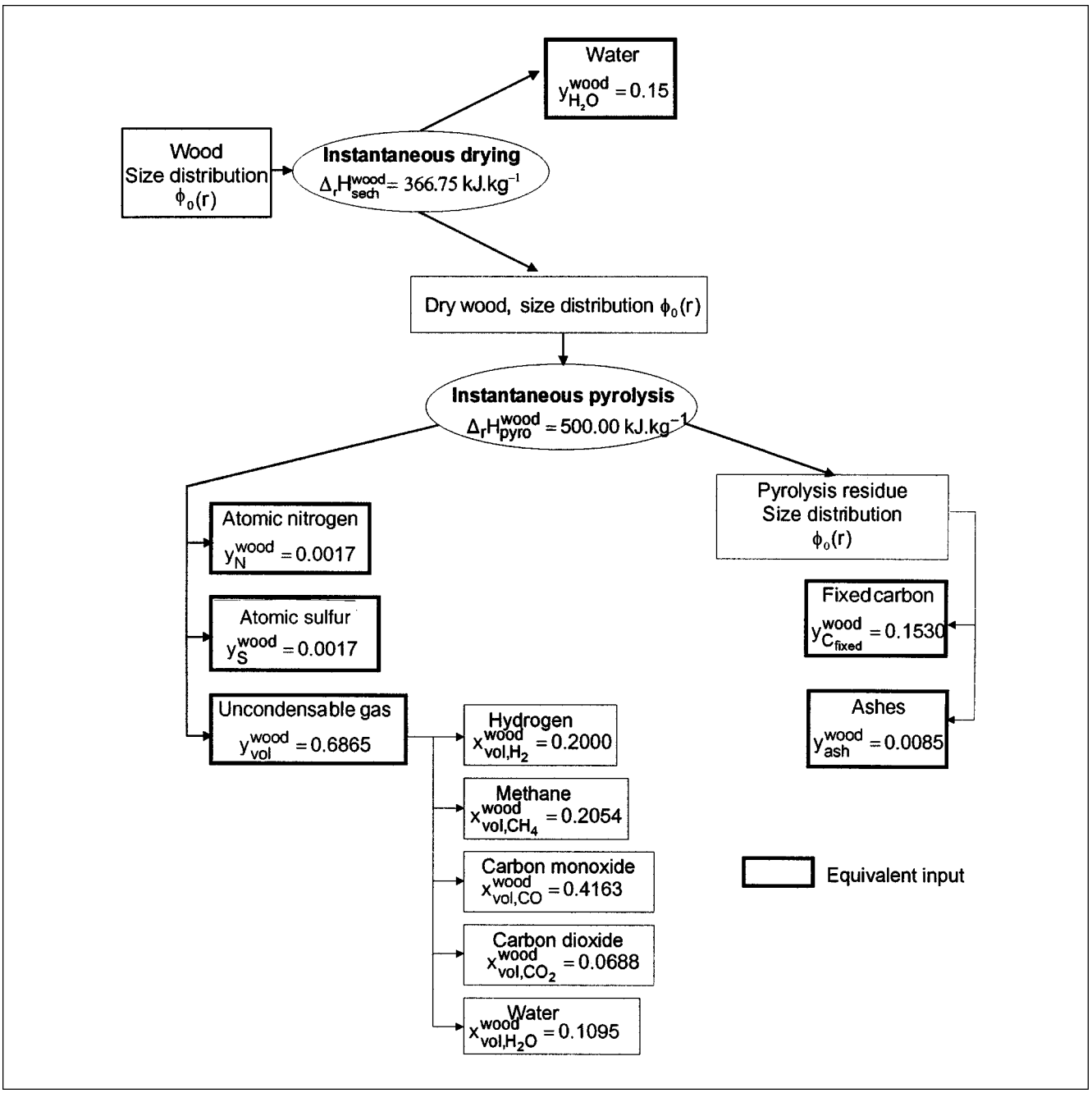

Figure 1. Flash pyrolysis of wood.

the ratio between mass fraction of volatile and carbon particles is quite different in both cases. As will be described in this section, a modified Werther's (1980) model is used to describe the hydrodynamic behavior of the bubbling bed. This model is completed to take into account phenomena occurring in the freeboard.

Hydrodynamics

Several models for the hydrodynamic description of a bubbling fluidized bed exist (as cited in the introduction) and have been used to model coal combustion. Moreover, because of the high volatility of municipal waste, hydrodynamic modeling must include work relative to volatile combustion in a fluidized bed (Stubington and Davidson, 1981; Turnbull and Davidson, 1984; Stubington and Chan, 1990, 1993; Clough and Stubington, 1995). The modeling effort should include all of the past advances which have been formulated by the different authors. Nevertheless, in order to reduce the CPU time requirements of a simulation, a cruder description has been formed of the hydrodynamic, but this includes the most significant phenomena.

Because of the high volatile content, incineration of municipal waste is mainly driven by diffusional combustion of

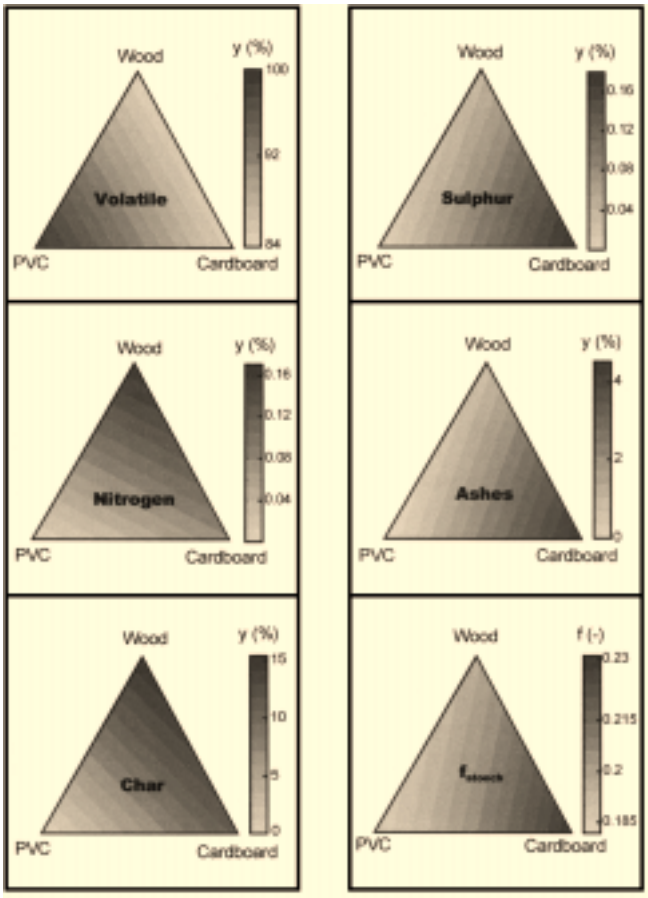

Figure 2. Composition of the equivalent input.

Mass ratio of products flow rate vs. initial waste composition. Value of the mixture fraction at stoichiometric conditions vs. initial waste composition.

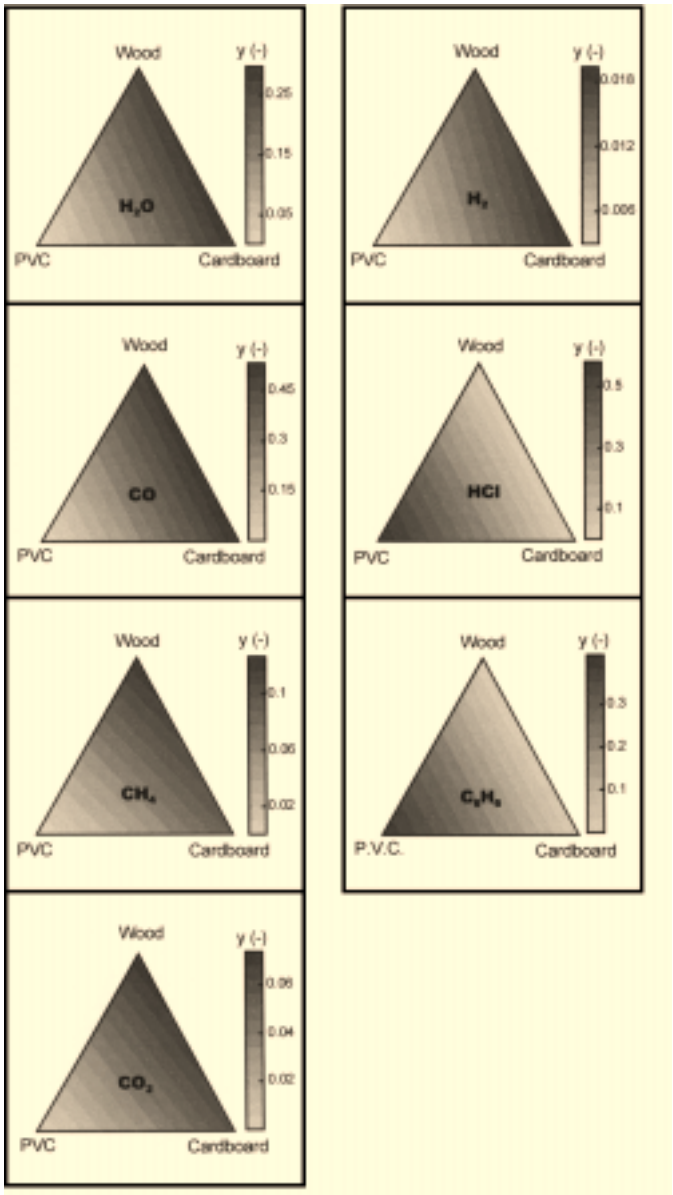

Figure 3. Composition of the gaseous equivalent input.

Mass fraction of named species vs. initial waste composition.

volatile. Consequently, Werther's (1980) model is very attractive because it assumes the existence of a film between the bubble and emulsion phase. This zone, placed between fuel-rich (emulsion) and fuel-lean (bubbles) regions, is suitable for the description of diffusion phenomena. Nevertheless, in its original formulation, one of the specifics of waste incineration cannot be taken into account. Indeed, the high devolatilization rate expected in the emulsion phase, and the upholding of this phase at incipient fluidization conditions implies the volatile, generated in the emulsion, to be removed from the bed by the ascending bubbles. This removal creates a transverse flux in the reactive zone, referred to in the next part of this study as ''the buffer zone.'' Such a flux leads to a 2-D treatment of this region. At last, this devolatilization creates an increase in the superficial velocity of the bubbles. Figure 4 summarizes our choice about zone modeling of the bubbling bed and shows the first fitting parameter of the model which is the buffer zone thickness δ.

Modeling of the freeboard region is achieved using two perfectly stirred regions. The first one, located just above the bed, takes into account the presence of solid particles because of the bubbles bursting. This zone is called ''the disengagement'' and its height is fixed at the transport disengaging height (TDH). The amount of sand present in this perfectly

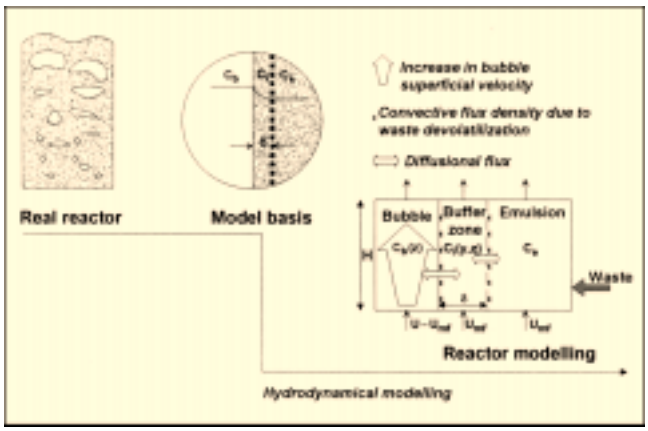

Figure 4. Bubbling bed model philosophy.

stirred region is evaluated from literature data (Milioli and Foster, 1995), and the second fitting parameter is the mass of carbonaceous particles present in terms of a fraction of the carbon load in the whole bed. Just above the disengagement, we find the post combustion zone which is devoted to homogeneous combustion and modeled as a perfectly stirred reactor.

The different assumptions used for the modeling of this modified Werther's model are shown in Table 2. Moreover, the mass-transfer characteristics are averaged over the whole bed, that is, both the local specific interfacial area and the mass-transfer coefficient are independent of height above the distributor and of the radial distance from the furnace center. The diffusion coefficient is the same for all the gaseous components present in the furnace and Schmidt's and Lewis's numbers are unity.

Finally, Figure 5 illustrates the complete model of the bed.

Gaseous mass and energy balances

In this part, the balances of chemical species and total enthalpy are presented. Because of the relevance of the buffer zone in our model, it has been selected for the mathematical transcription of the physical processes occurring in the reactor. With the aim of reducing the length of the main text, the main steps leading to such equations in the other zones of the model, as well as the equations themselves, are presented in the Appendix.

Enthalpy. The enthalpy is defined at a temperature T by the following equation

$$H^{\text{zone}} = \sum_{i=1}^{N} y_i^{\text{zone}} \left[h_{f,i}^{0}(T_{\text{ref}}) + \int_{T_{\text{ref}}}^{T} c_{p_i}(T)\, dT \right] \qquad (1)$$

Fluidizing Air Distribution. Let U be the superficial velocity of fluidizing air at atmospheric conditions (P_{atm}, T_{air}). Assuming the bubbling bed to be homogeneous in temperature, a relevant superficial velocity U_1 is defined (Eq. 2)

$$U_1 = U \frac{\rho_{\text{air}}(T_{\text{air}})}{\rho_{\text{emul}}(T_{\text{emul}})} \qquad (2)$$

This superficial velocity is used to quantify the amount of air entering each zone of the model in accordance with Werther's

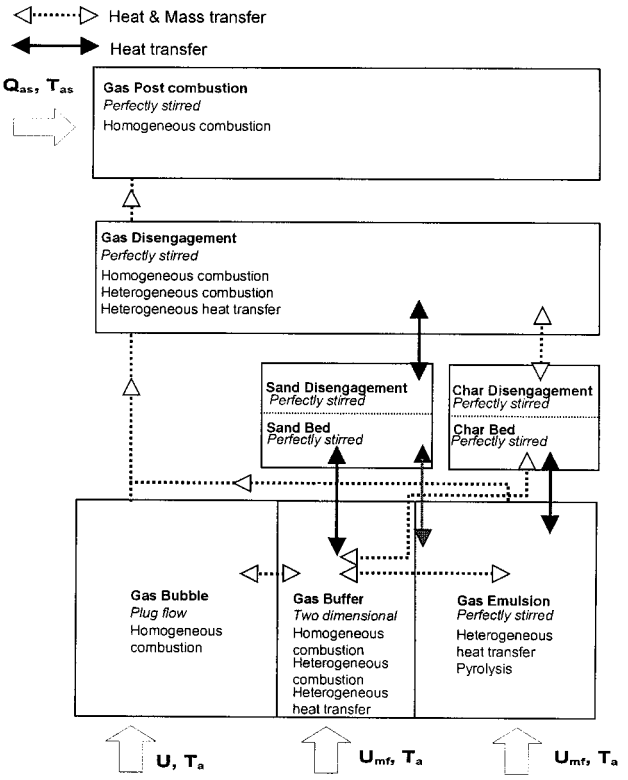

Figure 5. Overall furnace model.

Table 2. Different Assumptions Used for Modeling Modified Werther's Model

	Gas	Sand	Waste
Bubble	• Plug flow • Velocity: $U - U_{mf}$ • Increase of superficial velocity (transfer of volatile) • Constant combustion • Volatile combustion • Pollutant formation	• No sand	• No waste
Buffer	• Two dimensional • Velocity: U_{mf} • Constant density • Volatile combustion • Heterogeneous heat transfer • Heterogeneous combustion • Pollutant formation	• Diameter d_p • No attrition or thermal degradation • Perfectly stirred • Heterogeneous heat transfer	• Size distribution $\phi(r)$ • Perfectly stirred • Drying and pyrolysis • Heterogeneous heat transfer • Heterogeneous combustion • No influence on hydrodynamics
Emulsion	• Perfectly stirred • Velocity : U_{mf} • Constant density • Volatile combustion • Pollutant formation	• Diameter d_p • No attrition or thermal degradation • Perfectly stirred • Heterogeneous heat transfer	• Size distribution $\phi(r)$ • Perfectly stirred • Heterogeneous heat transfer • Heterogeneous combustion • No influence on hydrodynamics

(1980) first assumption

- Emulsion: $\dot{m}_{\text{air}}^{\text{emul}} = \rho_{\text{emul}} U_{\text{mf}}(T_{\text{emul}})\, A_c(1-a\delta)$, (3)
- Buffer zone: $\dot{m}_{\text{air}}^{\text{buff}} = \rho_{\text{emul}} U_{\text{mf}}(T_{\text{emul}})\, A_c a\delta$, (4)
- Bubble: $\dot{m}_{\text{air}}^{\text{bubb}} = \rho_{\text{emul}}\left[U_1 - U_{\text{mf}}(T_{\text{emul}})\right] A_c$. (5)

Buffer Zone. Let us consider a control volume of gas $a \times A_c \times \epsilon_{\text{mf}} \times dy \times dz$ in this zone. Four contributions might modify the rate of accumulation of a chemical species in this media (axial diffusion is neglected):

- The net transport of a species with ascending fluidizing air

$$\rho_{\text{emul}} a U_{mf}\, dy\left[\, y_k^{\text{buff}}(z) - y_k^{\text{buff}}(z+dz)\right]$$

- The net transport of a species by convective flow of volatile from emulsion to bubbles

$$\varphi_{\text{vol}}\, adz\left(\, y_k^{\text{buff}}(y+dy) - y_k^{\text{buff}}(y)\right)$$

where φ_{vol} denotes the specific mass flux of volatile from emulsion to bubbles

$$\varphi_{\text{vol}} = \frac{\dot{m}_{\text{vol}}}{a A_c L^{\text{bed}}} \tag{6}$$

- The net transport of a species by diffusion

$$-\rho_{\text{emul}} D a dz\left(\left.\frac{\partial y_k^{\text{buff}}}{\partial y}\right|_{y} - \left.\frac{\partial y_k^{\text{buff}}}{\partial y}\right|_{y+dy}\right)$$

- The net chemical reaction rate of a species

$$\epsilon_{\text{mf}}\, a dy dz R_k^{\text{buff}}$$

Given the rate of accumulation of a species in the control volume ϵ_{mf}dydz $[(\partial \rho_{\text{emul}} a y_k^{\text{buff}})/\partial t]$, the following balance equation is derived

$$\epsilon_{mf}\frac{\partial \rho_{\text{emul}} a y_k^{\text{buff}}}{\partial t} = -\rho_{\text{emul}} a U_{mf}(T_{\text{emul}})\frac{\partial y_k^{\text{buff}}}{\partial z} + \varphi_{\text{vol}} a\frac{\partial y_k^{\text{buff}}}{\partial y} + \rho_{\text{emul}} a D\frac{\partial^2 y_k^{\text{buff}}}{\partial y^2} + \epsilon_{mf} a R_{y_k}^{\text{buff}} \tag{7}$$

Fields of chemical species, as well as fields of total enthalpy, are supposed to be continuous from one zone to another. Thus, the following boundary conditions prevail

$$y_k^{\text{buff}}(y,\, z=0,t) = y_k^{\text{air}}(t);\; y_k^{\text{buff}}(y=0,z,t) = y_k^{\text{bubble}}(z,t);\; y_k^{\text{buff}}(y=\delta,z,t) = y_k^{\text{emul}}(t) \tag{8}$$

Moreover, at the outlet of the domain, it is supposed that there are no gradients in the axial direction

$$\left.\frac{\partial y_k^{\text{buff}}}{\partial z}\right|_{y,\, z=L^{\text{bed}}} = 0 \tag{9}$$

The same formalism, applied to total enthalpy, leads to an equivalent equation and boundary conditions.

Solid particles

Both sand and carbonaceous particles issued from pyrolysis are present in the bed. Sand is assumed to play a major role in the thermal homogenization. Carbonaceous particles also play an important role because they represent a particular fuel. Consuming oxygen and releasing heat both by heterogeneous combustion and convective heat transfer, the impact of carbon particles on species and enthalpy fields is of great importance.

Carbonaceous Particles. Estimation of chemical reaction rates and volumetric heat generation terms in gaseous balances requires parameters such as size distribution and rate of shrinkage of char particles. As previously assumed, carbonaceous particles enter the bed with the same size distribution as the initial waste ϕ_0.

Rate of Shrinkage. Char particles are expected to react either in the disengagement or in the buffer zone. Lack of oxygen in the emulsion and lack of particles in bubbles or post combustion prevent their combustion since it has been assumed that they burn the following reaction (Prins, 1987)

$$C + \Lambda O_2 \rightarrow (2-2\Lambda)CO + (2\Lambda - 1)CO_2, \quad \Lambda = 0.87 \tag{10}$$

Since we assume that the reaction takes place at the external surface of the particle, we have to quantify the area offered to the reaction and the corresponding oxygen concentration at every location of the furnace.

For example, a particle of radius r trapped in the disengagement would offer a total area $4\pi r^2$ to a reaction at a local oxygen concentration $[O_2]^{\text{dis}}$.

The situation is different for the same particle trapped in the buffer zone. Indeed, local oxygen concentration depends on the location of that particle.

However, there is one remaining problem: how can we know whether that particle is trapped within the control volume of the buffer zone, the emulsion, or the disengagement? A rigorous processing should imply a Lagrangian frame of reference for that particle. Such a following is not obvious in fluidized-bed systems. That is why we have chosen to use a concept based on mass and zone volume averaging.

We assumed that bursting of bubbles at the freeboard not only leads to sand projection within the disengagement, but to char particle projection also. Thus, a fraction α of the whole carbon load of the furnace is trapped within the disengagement. Focussing on our particle of radius r, we assumed that a fraction α of its external surface was in the disengagement and its remaining surface was in the buffer-emulsion system. In the same manner, we break this (1-α) fraction of the external surface into two parts. On a volume averaged basis, one portion is in the emulsion and another portion is in

the control volume of the buffer zone. To sum up, we can write that, for a particle of radius r, its external surface is divided into three parts:

- $S^{\text{dis,part}} = \alpha 4\pi r^2$ with a local oxygen concentration $[O_2]^{\text{dis}}$
- $dS^{\text{buff,part}} = (1-\alpha)\dfrac{a dydz}{L^{\text{bed}}(1-\epsilon_b)} 4\pi r^2$ with a local oxygen concentration $[O_2]^{\text{buff}}$
- $S^{\text{buff,part}} = (1-\alpha)\dfrac{1-\epsilon_b - a\delta}{(1-\epsilon_b)} 4\pi r^2$ with a nil local oxygen concentration.

Because the surface reaction (Eq. 10) is expected to be both kinetic and external transfer limited, the general expression for the reaction rate (per unit area) of the particle is

$$R_s^{\text{local}}(r) = \left[\frac{M_C k_s(r) k_m(r)}{\Lambda k_s(r) + k_m(r)}\right][O_2]^{\text{local}} \tag{11}$$

The external transfer coefficient $k_m(r)$ is evaluated following Prins's (1987) work

$$\epsilon_{mf}\frac{k_m(r)Sc^{2/3}}{U_{mf}} Re_{mf,p}^{n}(r) = 0.105 + 1.505\left(\frac{2r}{d_{\text{sand}}}\right)^{-1.505}$$

$$n = 0.35 + 0.29\left(\frac{2r}{d_{\text{sand}}}\right)^{-0.5} \tag{12}$$

Its evaluation does not require any other data about the particle. The case of the kinetic constant of the first-order reaction is slightly different. Indeed, its computation requires the particle temperature (Sriramulu et al., 1996)

$$k_s(r) = 595 T_C(r)\left[\frac{-149{,}220}{RT_C(r)}\right] \tag{13}$$

Assuming the Biot number of the particle to be lower than one, it is thermally homogeneous. Thus, a heat balance on the particle leads to

$$\frac{4}{3}\pi r^3 \frac{\partial \rho_C c_{p_C} T_C(r)}{\partial t}$$
$$= -\left[(1-\alpha)\frac{a}{L^{\text{bed}}(1-\epsilon_b)}\int_0^{L^{\text{bed}}}\int_0^{\delta}\left[R_s^{\text{buff}}(r)\right]dydz + \alpha R_s^{\text{dis}}(r)\right]4\pi r^2 \Delta_r H_C + \alpha h(r)\left[T^{\text{dis}} - T_C(r)\right]4\pi r^2$$
$$+ (1-\alpha)\frac{a h(r) 4\pi r^2}{L^{\text{bed}}(1-\epsilon_b)}\int_0^{L^{\text{bed}}}\int_0^{\delta}\left[T^{\text{buff}} - T_C(r)\right]dydz$$
$$+ (1-\alpha)h(r)\left[T^{\text{emul}} - T_C(r)\right]\frac{(1-\epsilon_b - a\delta)}{(1-\epsilon_b)}4\pi r^2 \tag{14}$$

Evaluation of the heat-transfer coefficient by Prins's (1987) relation (Eq. 15) requires some physical properties (such as thermal conductivity of gas, viscosity, and density), and temperature of the surrounding media. For simplicity, all these values have been computed at emulsion properties and assuming the Lewis and Schmidt numbers to be unity. Thus, there is only one value for the coefficient studied $h(r)$

$$\text{NuAr}^{-0.105} f_T^{-1} = 3.539 \qquad f_T = 0.844 + 0.0756 T/273 \tag{15}$$

Introducing the average oxygen molar concentration and temperature within the buffer as follows

$$\overline{[O_2]^{\text{buff}}} = \frac{1}{L^{\text{bed}}\delta}\int_0^{L^{\text{bed}}}\int_0^{\delta}[O_2]^{\text{buff}}dydz$$

$$\overline{T^{\text{buff}}} = \frac{1}{L^{\text{bed}}\delta}\int_0^{L^{\text{bed}}}\int_0^{\delta}T^{\text{buff}}dydz \tag{16}$$

one can compute the average reaction rate $\overline{R_s^{\text{buff}}(r)}$, which is the reaction rate in the buffer evaluated at mean oxygen concentration. These simplifications lead to

$$\frac{4}{3}\pi r^3 \frac{\partial \rho_C c_{p_C} T_C(r)}{\partial t}$$
$$= -\left[(1-\alpha)\frac{a\delta}{(1-\epsilon_b)}\overline{R_s^{\text{buff}}(r)} + \alpha R_s^{\text{dis}}(r)\right]4\pi r^2 \Delta_r H_C + \alpha h(r)\left[T^{\text{dis}} - T_C(r)\right]4\pi r^2$$
$$+ (1-\alpha)\frac{a\delta 4\pi r^2}{(1-\epsilon_b)}h(r)\left[\overline{T^{\text{buff}}} - T_C(r)\right]$$
$$+ (1-\alpha)h(r)\left[T^{\text{emul}} - T_C(r)\right]\frac{(1-\epsilon_b - a\delta)}{(1-\epsilon_b)}4\pi r^2 \tag{17}$$

Once this balance is solved, the particle temperature is available, and the rate of shrinkage of a particle can easily be derived

$$\omega(r) = \frac{-1}{\rho_C}\left(\frac{M_C k_s(r) k_m(r)}{\Lambda k_s(r) + k_m(r)}\right)\left[(1-\alpha)\frac{a\delta}{(1-\epsilon_b)}\overline{[O_2]^{\text{buff}}} + \alpha[O_2]^{\text{dis}}\right] \tag{18}$$

Population Balance. This balance takes into account carryover, elutriation, and shrinkage, and is derived from the Kunii and Levenspiel (1991) differential equation for size distribution of carbonaceous particles inside the bed

$$F_0\phi_0(r) - F_1\phi(r) - F_2\phi(r)dr - W_C\frac{d}{dr}[\omega(r)\phi(r)] + \frac{3W_C\phi(r)}{r}\omega(r) = 0 \tag{19}$$

This equation requires the carbon load in the bed (W_C) to be known. Such an unknown is the result of the normalization Eq. 20

$$\int_0^{r_{\max}}\phi(r)dr = 1 \tag{20}$$

In the above expressions, F_0, F_1, and F_2 point out, respectively, the mass-flow rate of carbonaceous particles issued from pyrolysis, the mass-flow rate carryover, and the mass-flow rate elutriated computed by relation 21 (Wen and Hashinger, 1960)

$$\frac{F_2(r)}{gA_c(U-U_t(r))} = 1.7.10^{-5}\left(\frac{(U-U_t(r))^2}{2gr}\right)^{0.5} \times\left(\frac{2rU_t(r)\rho_{\text{emul}}}{\mu_{\text{emul}}}\right)^{0.725}\left(\frac{\rho_c-\rho_{\text{emul}}}{\rho_{\text{emul}}}\right)^{1.15}\left(\frac{U-U_t(r)}{U_t(r)}\right)^{0.10} \tag{21}$$

Sand Particles. In fluidized-bed combustion systems, some sand is elutriated. However, in order to ensure the quality of fluidization, its mass must be kept constant within the furnace. Thus, there is a continuous supply of this material. As a consequence, for our modeling purposes, we assume the mass of sand W_{sand} to be constant. Of course, this material is subject to attrition phenomena, which lead to a modification in its size distribution. As a simplification, we suppose that its diameter d_{sand} is constant.

Bursting of the bubbles at the freeboard of the bed carries sand in the disengagement. Thus, the thermal level of the disengagement is strongly affected by the presence of this material. That is why the quantification of the amount of sand present in this region is required. Following the work of Milioli and Foster (1995), the mass-flow rate of sand carried by bursting of bubbles is

$$F_w = 0.1\,A_c\,\rho_{\text{sand}}(1-\epsilon_{mf})U(L^{\text{bed}}) \tag{22}$$

Moreover, assuming that the resident time of a particle present in this region is computed using its terminal velocity, one is able to evaluate its sand content (Eq. 23)

$$W_{\text{sand}}^{\text{dis}} = \frac{0.1\,A_c\,\rho_{\text{sand}}(1-\epsilon_{mf})U(L^{\text{bed}})L^{\text{dis}}}{U_t} \tag{23}$$

Thermal levels within the furnace are strongly affected by heterogeneous convective transfer with sand. Quantification of this heat generation requires the particle temperature to be known. Using the same concept of mass and volume averaging used in the case of reacting particles, one can compute the area offered to transfer with sand within each region of the furnace

- $S^{\text{dis,sand}} = \dfrac{W_{\text{sand}}^{\text{dis}}}{W_{\text{sand}}}\pi d_{\text{sand}}^2$,
- $dS^{\text{buff,sand}} = \left(\dfrac{W_{\text{sand}}^{\text{dis}}-W_{\text{sand}}^{\text{dis}}}{W_{\text{sand}}^{\text{dis}}}\right)\dfrac{adydz}{L^{\text{bed}}(1-\epsilon_b)}\pi d_{\text{sand}}^2$
- $S^{\text{buff, sand}} = \left(\dfrac{W_{\text{sand}}-W_{\text{sand}}^{\text{dis}}}{W_{\text{sand}}}\right)\dfrac{1-\epsilon_b-a\delta}{(1-\epsilon_b)}\pi d_{\text{sand}}^2$

Evaluation of the heat-transfer coefficient by Prins's (1987) relation (Eq. 15) is performed using emulsion properties. Thus, there is only one value for the coefficient h. The formulation of the heat balance on a sand particle leads to

$$\frac{\rho_{\text{sand}}c_{p_{\text{sand}}}\pi d_{\text{sand}}^3}{6}\frac{\partial T_{\text{sand}}}{\partial t} = \left(\frac{W_{\text{sand}}-W_{\text{sand}}^{\text{dis}}}{W_{\text{sand}}}\right)\pi d_{\text{sand}}^2\frac{1-\epsilon_b-a\delta}{(1-\epsilon_b)}h(T^{\text{emul}}-T^{\text{sand}}) + \left(\frac{W_{\text{sand}}-W_{\text{and}}^{\text{dis}}}{W_{\text{sand}}}\right)\pi d_{\text{sand}}^2 \frac{a}{L^{\text{bed}}(1-\epsilon_b)}\int_0^{L^{\text{bed}}}\int_0^{\delta}h(T^{\text{buff}}-T^{\text{sand}})\text{dydz} + \left(\frac{W_{\text{sand}}^{\text{dis}}}{W_{\text{sand}}}\right)\pi d_{\text{sand}}^2 h(T^{\text{dis}}-T^{\text{sand}}) \tag{24}$$

Using the previously defined average buffer temperature (Eq. 16), this equation becomes

$$\frac{\rho_{\text{sand}}c_{p_{\text{sand}}}d_{\text{sand}}}{6}\frac{\partial T_{\text{sand}}}{\partial t} = \left(\frac{W_{\text{sand}}-W_{\text{sand}}^{\text{dis}}}{W_{\text{sand}}}\right)\frac{1-\epsilon_b-a\delta}{(1-\epsilon_b)}h(T^{\text{emul}}-T^{\text{sand}}) + \left(\frac{W_{\text{sand}}-W_{\text{sand}}^{\text{dis}}}{W_{\text{sand}}}\right)\frac{a\delta}{(1-\epsilon_b)}h(\overline{T^{\text{buff}}}-T^{\text{sand}}) + \left(\frac{W_{\text{sand}}^{\text{dis}}}{W_{\text{sand}}}\right)h(T^{\text{dis}}-T^{\text{sand}}) \tag{25}$$

Chemical reaction rate and volumetric heat generation

Balance equations have been written for each of the parts of the modeled incinerator. Nevertheless, chemical reaction rate and volumetric heat generation of those equations have not been detailed because of insufficient knowledge concerning solid particles. These source terms are presented here for the case of the buffer zone, with the other ones being given in the appendix.

According to the model assumptions, only three contributions are taken into account in the source terms of any region of the modeled reactor. They are: homogeneous combustion of volatile; heterogeneous combustion of carbon particles; and heat transfer with sand and char.

Equations describing conservation of gaseous pollutants (NO, HCN, S, SO_2, SO_3) are the same as those written previously. Nevertheless, an explanation will be given as to how source terms occurring in these equations are computed.

Chemical Reaction Rate. Because the kinetic rates involved by volatile combustion are very high, chemical equilibrium is assumed to control conversion. Thus, as explained in this section, both the mixture fraction concept and the minimization of Gibb's free energy are used to compute the result of this combustion.

Dealing with combustion of carbon particles, and because of the choice of the heterogeneous reaction (Eq. 10) only

three gaseous chemical species are involved, namely O_2, CO and CO_2.

Given the size distribution $\phi(r)$ of the carbon pellets inside the bed, the number of these pellets, of which the radius is between r and $r + dr$, and present in the emulsion-buffer system is

$$N^{\text{buff}}(r) = (1-\alpha)\frac{3W_C\phi(r)dr}{4\pi\rho_C r^3} \tag{26}$$

Assuming equiprobability for the position of a particle inside this system, one is able to evaluate the number of these particles present in the control volume of the buffer

$$N^{\text{buff},C.V.}(r) = (1-\alpha)\frac{3W_C\phi(r)dr}{4\pi\rho_C r^3}\frac{aA_c dydz}{A_c L^{\text{bed}}(1-\epsilon_b)} \tag{27}$$

The computation of the area involved by the reaction inside this volume can then easily be derived

$$dS^{\text{buff,partic}}(r) = (1-\alpha)\frac{3aW_C\phi(r)dr}{r\rho_C L^{\text{bed}}(1-\epsilon_b)}dydz \tag{28}$$

Because of the choice of the surface reaction model, the chemical reaction rate can now be processed (in the case of oxygen for example), once all the radii of particles have been included

$$R_{O_2}^{\text{buff,partic}} = -(1-\alpha) \times \frac{3W_C M_{O_2}[O_2]^{\text{buff}}}{\rho_c A_c L^{\text{bed}}(1-\epsilon_b)\epsilon_{mf}}\int_0^{R_m}\frac{\Lambda k_m(r)k_s(r)\phi(r)}{[\Lambda k_s(r)+k_m(r)]_r}dr \tag{29}$$

Correspondingly, chemical reaction rates for carbon monoxide and dioxide are obtained using the stoichiometry of reaction (Eq. 10).

The concentration of pollutants inside the system are very small. Thus, their contribution to the chemical reaction rate of main compounds (O_2, N_2) is neglected. Pollutant formation only affects the chemical reaction rate of NO, HCN, SO_2 and SO_3. The method of computation is explained in the next section.

Volumetric Heat Generation. The choice has been made to represent the energy level of the system through total enthalpy. Thus, there is no contribution of volatile combustion to the total enthalpy balance. As pollutant formation is neglected in the chemical reaction rate of main compounds, total enthalpy in the control volume is only affected by reacting particles and heterogeneous heat transfer with the solids. Because of the definition of the total enthalpy, the contribution of the reacting particles arises through standard enthalpy of formation of solid carbon and external heat transfer

$$R_H^{\text{buff,part}} = \frac{\beta}{\Lambda}R_{O_2}^{\text{buff,part}}h_{f,C}^0 + (1-\alpha)\frac{3W_C}{\rho_C A_C L^{\text{bed}}\epsilon_{mf}(1-\epsilon_b)} \times \int_0^{R_m}\frac{h(r)\left[T_C(r)-T^{\text{buff}}\right]\phi(r)}{r}dr \tag{30}$$

Assuming the equiprobability of the presence of sand particles (held in the bubbling bed) within the buffer-emulsion system, one is able to estimate the area offered to convective heat transfer in the control volume

$$dS^{\text{buff,sand}} = \frac{6\left(W_{\text{sand}}-W_{\text{sand}}^{\text{dis}}\right)}{\rho_{\text{sand}}d_{\text{sand}}}\frac{adydz}{(1-\epsilon_b)L^{\text{bed}}} \tag{31}$$

Then, the volumetric heat generated by convective transfer with sand can easily be derived

$$R_H^{\text{buff,sand}} = \frac{6\left(W_{\text{sand}}-W_{\text{sand}}^{\text{dis}}\right)}{\rho_{\text{sand}}d_{\text{sand}}\epsilon_{mf}A_c(1-\epsilon_b)L^{\text{bed}}}h(T^{\text{sand}}-T^{\text{buff}}) \tag{32}$$

The total heat released within a control volume of the buffer zone is the sum of the two previous ones

$$R_H^{\text{buff}} = R_H^{\text{buff,part}} + R_H^{\text{buff,sand}} \tag{33}$$

Pollutants

Two classes to pollutants are discussed here: nitrogenous and sulfurous.

Nitrogenous Pollutants: Use of Kinetic Laws. The model developed here provides a tool to understand the source of NO_x production in a fluidized-bed incineration process via thermal and fuel-bond mechanism.

To predict NO_x emission, the model solves a transport equation for both nitric oxide (NO) and hydrogen cyanide (HCN) mass fractions. These transport equations are solved based on a given flow, species, and temperature fields solutions. In other words, NO_x is post-processed from a combustion simulation.

The source terms occurring in any of these equations are to be determined next, taking into account the NO_x mechanism: thermal and fuel-bound NO_x.

Thermal NO_x. The formation of thermal NO_x is determined by a set of highly temperature-dependent chemical reactions known as the extended Zeldovich mechanism. The principal reactions governing the formation of thermal NO_x from molecular nitrogen are as follows (Chigier, 1981; Glassman, 1996)

$$O + N_2 \overset{k_1}{\longleftrightarrow} N + NO \tag{34}$$

$$N + O_2 \overset{k_2}{\longleftrightarrow} O + NO \tag{35}$$

$$N + OH \overset{k_3}{\longleftrightarrow} H + NO \tag{36}$$

The rate constants for these reactions are reported in Table 3 (Hanson and Salimian, quoted in Fluent 5 User's Guide (1998), both for forward and reverse reactions. Using well known assumptions (Chigier, 1981; Glassman, 1996), the NO chemical reaction rate, due to thermal NO_x mechanism, is

Table 3. Rate Constants for Thermal NO_x Mechanism Hanson and Salimian, Quoted in Fluent 5 User's Guide (1998)

Reaction		Rate Constant ($m^3 \cdot mol^{-1} \cdot s^{-1}$)
(34)	Forward	$k_1 = 1.8\times10^8 \exp\left(\frac{-38{,}370}{T}\right)$
	Reverse	$k_{-1} = 3.8\times10^7 \exp\left(\frac{-425}{T}\right)$
(35)	Forward	$k_2 = 1.8\times10^4 T \exp\left(\frac{-4{,}680}{T}\right)$
	Reverse	$k_{-2} = 3.8\times10^3 T \exp\left(\frac{-20{,}820}{T}\right)$
(36)	Forward	$k_3 = 7.1\times10^7 \exp\left(\frac{-450}{T}\right)$
	Reverse	$k_{-3} = 7.1\times10^8 \exp\left(\frac{-24{,}560}{T}\right)$

computed in any region of the model through relation 37 and 38

$$R_{\text{thermal,NO}} = M_{\text{NO}} \frac{2[\text{O}]\left(k_1 k_2 [\text{O}_2][\text{N}_2] - k_{-1} k_{-2} [\text{NO}]^2\right)}{k_2[\text{O}_2] + k_{-1}[\text{NO}]} \tag{37}$$

$$[\text{O}] = 36.64 T^{1/2} [\text{O}_2]^{1/2} \exp\left(\frac{-27{,}123}{T}\right) (\text{mol}\cdot\text{m}^{-3}) \tag{38}$$

Fuel-Bound NO. The nitrogen-containing organic compounds, present in the initial waste (wood and cardboard) contribute to the total NO_x formed during the incineration process. It was assumed previously that during the pyrolysis step, atomic nitrogen was produced from wood and cardboard.

The route leading to fuel NO_x formation and destruction can be summed up by the simplified model (De Soete, 1975; Chigier, 1981; Glassman, 1996)

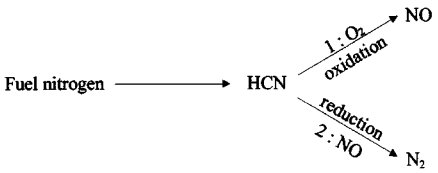

The chemical reaction rate in the hydrogen cyanide balance can be computed through relation 41

$$R^1_{\text{HCN}} = -A_1 \left(\frac{RT}{P_{\text{atm}}}\right)^a \exp\left(\frac{-E_1}{RT}\right) M_{\text{HCN}} [\text{HCN}][\text{O}_2] \tag{39}$$

$$R^2_{\text{HCN}} = -A_2 \left(\frac{RT}{P_{\text{atm}}}\right) \exp\left(-\frac{E_2}{RT}\right) M_{\text{HCN}} [\text{HCN}][\text{NO}] \tag{40}$$

$$R_{\text{HCN}} = R^1_{\text{HCN}} + R^2_{\text{HCN}} \tag{41}$$

The different constants occurring in the last equation are given in Table 4 (De Soete, 1975). The corresponding source terms occurring in nitric oxide conservation equations can be computed through stoichiometric relations (Eq. 42)

$$R_{\text{fuel,NO}} = \frac{M_{\text{NO}}}{M_{\text{HCN}}} \left(R^1_{\text{HCN}} - R^2_{\text{HCN}}\right) \tag{42}$$

Finally, the source term for nitric oxide arising in any of its conservation equations is computed by adding its thermal and fuel contribution.

Sulfurous Pollutants: Use of Chemical Equilibrium. As sulfur is contained in the initial waste, both SO_2 and SO_3 are produced in the incinerator. Computing their respective mass fraction fields is achieved using chemical equilibrium between S, O_2, SO_2, and SO_3. As in the case of NO_x, SO_x emissions are computed in a post processing step once temperature and stable species fields have been evaluated. In order to perform the equilibrium calculation, the first step is to solve the transport equation for the sulfur element.

Once elemental sulfur mass fraction fields have been computed, equilibrium calculations are performed following the reactions 43 and 44 (Chigier, 1981; Glassman, 1996)

$$\text{S} + \text{O}_2 \longleftrightarrow \text{SO}_3 \tag{43}$$

$$\text{SO}_2 + \frac{1}{2}\text{O}_2 \longleftrightarrow \text{SO}_3 \tag{44}$$

Equilibrium constants are computed using standard enthalpy and entropy of this species and using the relation (Eq. 45).

$$\Delta_r G^0(T) + RT \ln K(T) = 0 \tag{45}$$

Table 4. Constants in Eqs. 39 and 40 (De Soete, 1975)

Reaction	Preexponential factor (s^{-1})	Activation Energy ($J\cdot m^{-1}$)	Exponent
Oxidation	$A_1 = 3.5\times10^{10}$	$E_1 = 280515$	$a = \begin{cases} 1.0, & x_{\text{O}_2} \le 4.1\times10^{-3} \\ -3.95 - 0.9 \ln x_{\text{O}_2}, & 4.1\times10^{-3} \le x_{\text{O}_2} \le 1.11\times10^{-2} \\ -0.35 - 0.1 \ln x_{\text{O}_2}, & 1.11\times10^{-2} \le x_{\text{O}_2} \le 0.03 \\ 0, & x_{\text{O}_2} \ge 0.03 \end{cases}$
Reduction	$A_2 = 3.5\times10^{12}$	$E_2 = 251208$	

The PrePDF code of the Fluent 5 package yields the set of thermodynamic properties (standard enthalpy and entropy, and constant-pressure specific heats).

At this step, the overall model of the fluidized-bed incineration process is given. However, in order to reduce CPU time requirement, further assumptions are needed.

Resolving of the Overall Model

As a first attempt, only a steady-state operation is performed. In the previous paragraph, a distinction was made between the chemical reaction rate and volumetric heat generation arising from volatile and char combustion. This distinction is a consequence of the high volatile content of the initial waste. A superimposition technique has been used to solve the overall problem. In the first instance, balance equations are solved by neglecting char combustion. The resolving of the subsequent simplified balances leads to gaseous chemical species mass fraction y_k^{vol} and temperature T^{vol}. Secondly, variations in these fields, respectively, Δy_k and ΔT, are computed, assuming these variations to be small enough to remain volatile chemical reaction rate and volumetric heat generation at their initial value

$$R_k^{\text{zone,vol}}\left(y_k^{\text{vol}}+\Delta y_k, T^{\text{vol}}+\Delta T\right)=R_k^{\text{zone,vol}}\left(y_k^{\text{vol}}, T^{\text{vol}}\right) \quad (46)$$

$$\dot{Q}^{\text{zone,vol}}\left(y_k^{\text{vol}}+\Delta y_k, T^{\text{vol}}+\Delta T\right)=\dot{Q}^{\text{zone,vol}}\left(y_k^{\text{vol}}, T^{\text{vol}}\right) \quad (47)$$

These variations are superimposed on previous fields, in so doing leading to new ones, which are used to compute pollutants fields in third stage.

The first step: volatile combustion

With the exception of pollutants, the gaseous mixture is composed of nine species. Resolving their equations in each zone of the model would require lengthy computer processing time and data storage. In order to diminish these requirements, the mixture fraction concept (Kuo, 1986; Borghi and Destriau, 1995; Turns, 1996) has been used. Under the assumption that there is an equal diffusion coefficient for every gaseous species, it allows the thermochemical state of the gas to be described perfectly, given mixture fraction f and total enthalpy H. Links between these two data, temperature, and species mass fraction are obtained from tables resulting from chemical computation. Such a link is given on Figure 6, which represents temperature level as a function of f and H. The other advantage of using the mixture fraction concept is the conservative nature of f. As a consequence, the balance equation for mixture fraction is devoid of any source term. The following balance equations can then be derived in the buffer zone

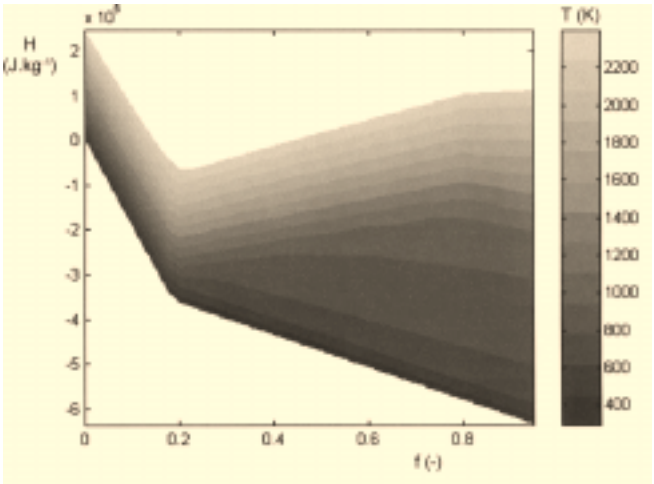

Figure 6. Area plot of mixture fraction, total enthalpy and temperature link.

$$-\rho_{\text{emul}} a U_{mf}(T_{\text{emul}})\frac{\partial f}{\partial z}+\varphi_{\text{vol}} a\frac{\partial f}{\partial y}+\rho_{\text{emul}} aD\frac{\partial^2 f}{\partial y^2}=0 \quad (48)$$

$$-\rho_{\text{emul}} a U_{mf}(T_{\text{emul}})\frac{\partial H^{\text{buff}}}{\partial z}+\varphi_{\text{vol}} a\frac{\partial H^{\text{buff}}}{\partial y}+\rho_{\text{emul}} aD\frac{\partial^2 H^{\text{buff}}}{\partial y^2}+\epsilon_{mf} aR_H^{\text{buff,sand}}=0 \quad (49)$$

Two major numerical difficulties arise in the resolving of this part of the model. The first one is related to the differential nature of the balance equations within two zones of the model. A finite volume method has been used to convert these into an algebraic matrix system. The second is inherent in coupling between zones, which occurs both from boundary conditions and sand-dependent volumetric heat generation. These couplings require the general algorithm of resolution to be iterative. However, because of the strength of the thermal coupling, a relaxation method had to be used in order to avert the numerical instabilities that it involved.

Because of the total enthalpy source terms and because of the dependence of physical properties with temperature, sand and zone temperatures are required at each step of the iteration scheme. These temperatures can be computed from f and H values using a double interpolation scheme. Nevertheless, such interpolations drastically reduce the speed of the convergence of the algorithm. Increasing this speed has been performed using a two-hidden-layer tangent sigmoid neural network. Each hidden layer is composed of eight neurons and the network is trained using Levenberg Marquardt algorithm (quoted in Matlab, Neural Network Toolbox User's Guide (1998)). The task of this trained network is to yield the temperature of the different zones given a vector containing all the f and H couples.

Figure 7 shows the general algorithm of resolution of volatile combustion. Once convergence is reached, the double interpolation scheme is used to obtain species mass fractions fields.

Second step: Carbon particles combustion

Following the assumptions 46 and 47 formulated in this main section, balance equations for variations in O_2, CO, CO_2 ($\Delta y_k^{\text{local}}$) and total enthalpy ($\Delta H_k^{\text{local}}$) fields can be derived (only buffer balances are presented here)

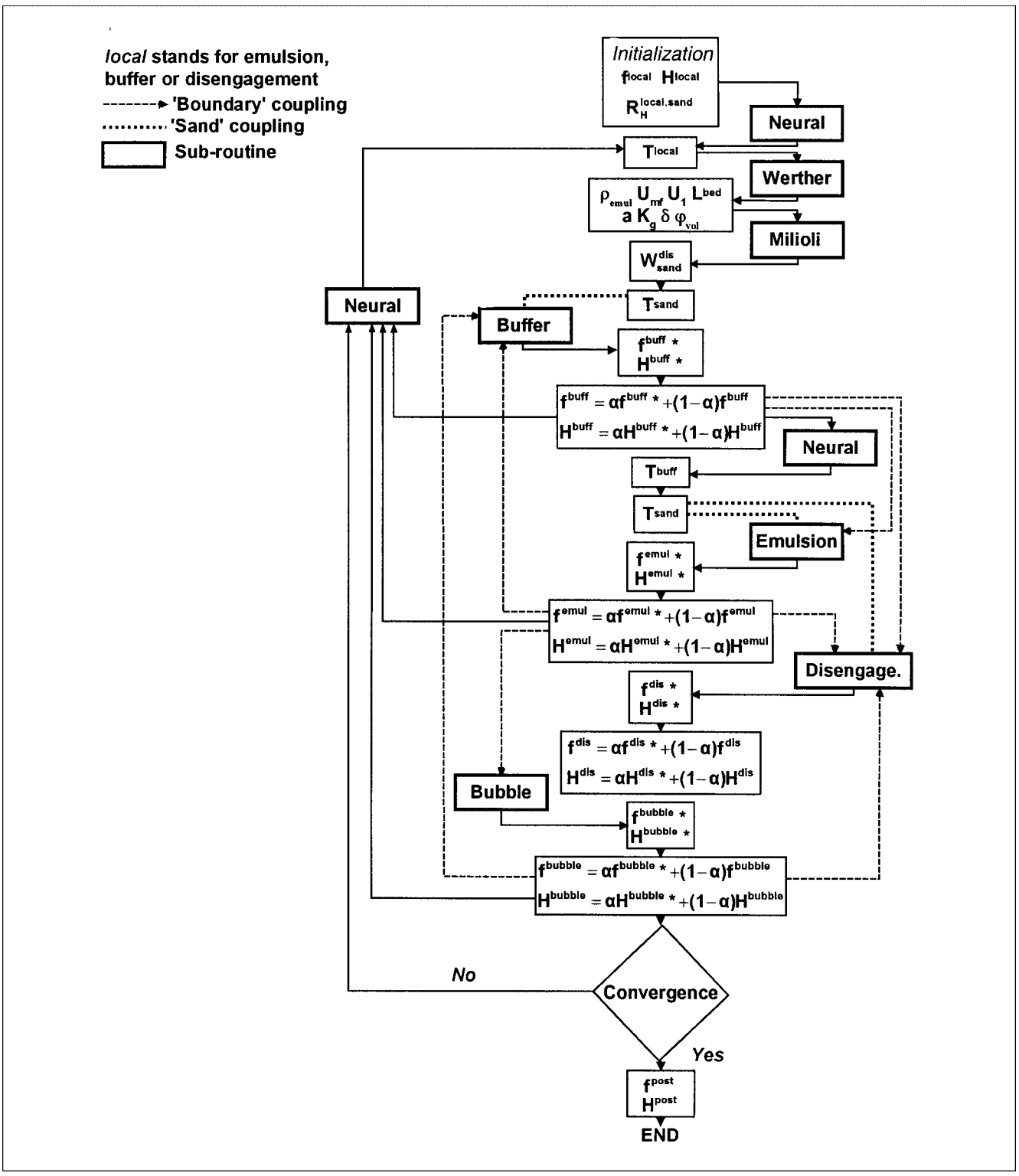

Figure 7. General algorithm of resolution of the model.

$$-\rho_{\text{emul}} a U_{mf}(T_{\text{emul}}) \frac{\partial \Delta y_k^{\text{buff}}}{\partial z} + \varphi_{\text{vol}} a \frac{\partial \Delta y_k^{\text{buff}}}{\partial y} + \rho_{\text{emul}} a D \frac{\partial^2 \Delta y_k^{\text{buff}}}{\partial y^2} + \epsilon_{mf} a R_{y_k}^{\text{buff,part}} = 0 \quad (50)$$

$$-\rho_{\text{emul}} a U_{mf}(T_{\text{emul}}) \frac{\partial \Delta H_k^{\text{buff}}}{\partial z} + \varphi_{\text{vol}} a \frac{\partial \Delta H_k^{\text{buff}}}{\partial y} + \rho_{\text{emul}} a D \frac{\partial^2 \Delta H_k^{\text{buff}}}{\partial y^2} + \epsilon_{mf} a R_H^{\text{buff,part}} = 0 \quad (51)$$

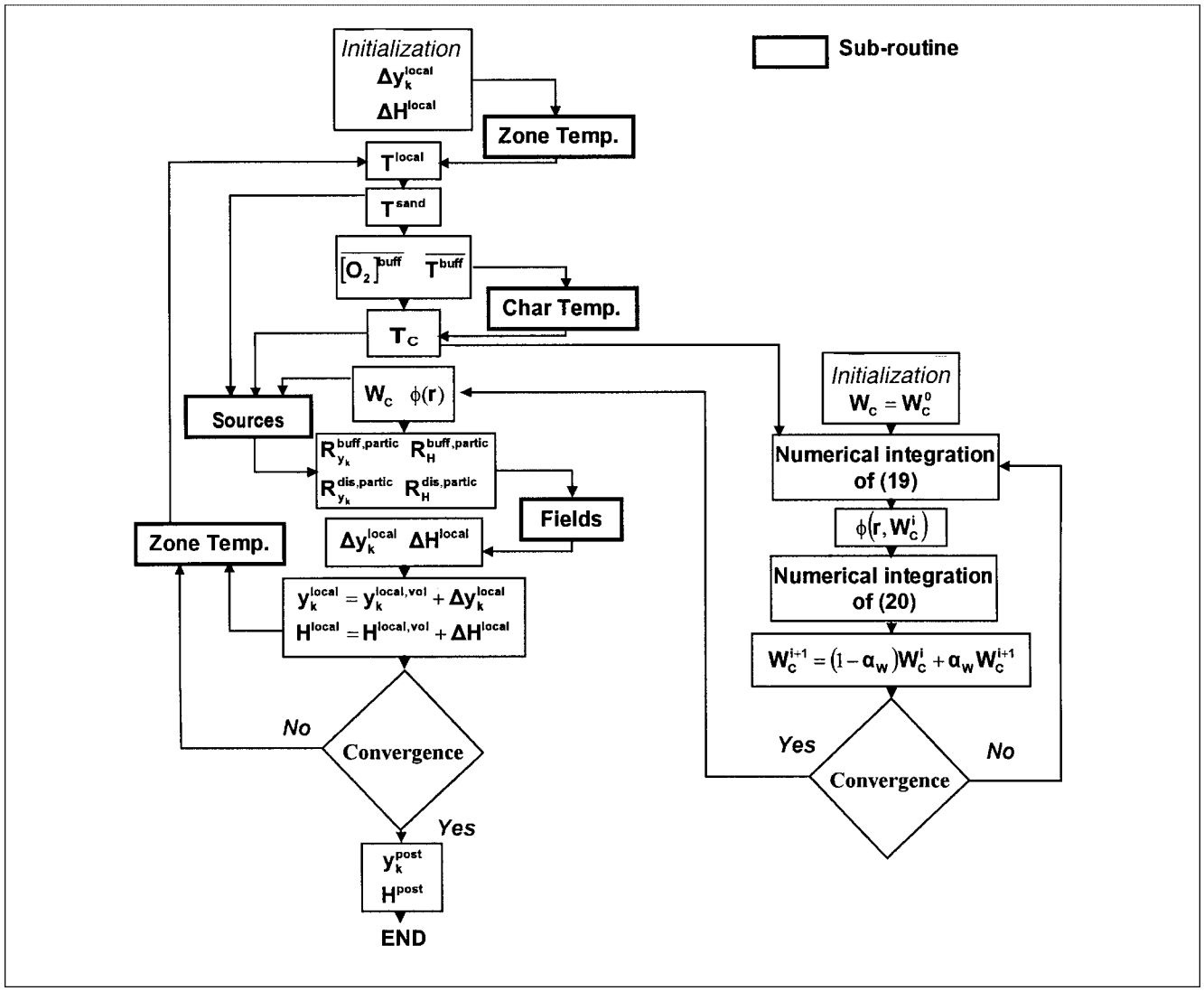

Figure 8. Algorithm of the reactive particle set of resolution.

Resolution of these balances is performed using a double iterative scheme (Figure 8). Given fields of temperature and oxygen mass fraction, one can compute carbon particle size distribution and carbon load using the Selçuk et al. (1996) algorithm. This size distribution allows computation of source terms arising in O_2, CO, CO_2, and H variation equations. Then, by using an iterative relaxation method, variations in these previous fields can be computed. This iterative scheme neglects effects of temperature variations on physical properties computed from volatile combustion. Once variations in O_2, CO, CO_2, and H fields have been evaluated, they are superimposed onto existing fields, providing initial conditions for the computation of new carbon particle-size distribution and carbon load in the bed.

Third step: pollutants formation

Temperature, nitrogen, and oxygen mass fraction fields have been definitively computed in the previous step. Computation of SO_x and NO_x mass fraction fields are successively performed using an iterative relaxation algorithm as in the case of volatile combustion.

Results

As an illustrating example, a typical incinerator of 1 MW is simulated. Geometrical settings involved for such a furnace as well as typical operating parameters used for simulation are given in Table 4. The influence of three operating parameters (superficial fluidization velocity, initial waste composition, and power evacuated by the in-bed boiler) is evaluated through simulations. As our strategy is to build a model for simulation and control, such influences can be drawn once fitting parameters (δ and α) have been fixed. In a rigorous study, such parameters would be deduced from experimental studies. However, we do not have such results at the moment. Thus, the parameters have been fixed as follows.

Table 5. Incinerator and Standard Operating Parameter Data

Incinerator Data	
Operating power	$P = 1$ MW
Equivalent dia. (square base)	$D = 0.5$ m
Total height	$L_{tot} = 8$ m
No. of orifices per square meter (distributor)	$n_{or} = 2500$
Sand Data	
Diameter	$d_{sand} = 10^{-3}$ m
Density	$\rho_{sand} = 2630$ kg·m^{-3}
Operating Parameters Used for Simulation	
Mass-flow rate of waste	$Q_w = 0.06$ kg·s^{-1}
Waste size distribution (normal law)	$R_{avg} = R_{max} = 1.5 \cdot 10^{-2}$ m $\sigma = 3.10^{-3}$ m
Waste initial temperature	$T_W = 298$ K
Outflow rate	$F_1 = 0$ kg·s^{-1}
Superficial velocity	$U = 1.3$ to 2.5 m·s^{-1}
Fluidizing air temperature	$T_a = 298$ K
Secondary air-flow rate	$\dot{m}^s_{air} = 0$ or 0.03 kg·s^{-1}
Secondary air temperature	$T_{as} = 298$ K
Power evacuated by the in-bed boiler	$P_{boil} = 0$ to 500 kW

Buffer zone thickness is linked to diffusion and mass-transfer coefficients through relation 52

$$\delta = \frac{D}{K_g} \tag{52}$$

An estimation of the overall mass-transfer coefficient (K_g) comes from Werther's work. Then, the buffer zone thickness is found through the diffusion coefficient value. For our purposes, the diffusion coefficient is fixed to 10^{-4} m^2·s^{-1}, which is an average value for the gaseous mixture at the temperature encountered in the incineration process (1,200 K).

Most of the air entering the bed crosses it through bubbles. That is why most of the air entering the bed is expected to be carried out in the freeboard. This explains why the mass ratio of carbon particles in the disengagement zone to that in the bed is of importance in the computing of carbon load of the furnace. Its value is fixed equal to the mass ratio of sand in the disengagement zone to that in the bed (Eq. 53)

$$\alpha = \frac{W^{dis}_{sand}}{W_{sand}} \tag{53}$$

The sensitivity analysis of these fitting parameters can be found elsewhere (Marias, 1999). As a summary, we can say that these parameters do not significantly modify the composition of the exhaust gas, but they strongly affect the carbon load. For instance, increasing the diffusion coefficient to a value of 1.5×10^{-4} m^2·s^{-1}, the exhaust gas composition remains unchanged whereas the carbon load is divided by a factor of 2.

Overall model result

Figure 7 illustrates typical results of computation, given a set of operating parameters (Table 2, $U = 1.9$ m·s^{-1}, $T_{air} = 298$ K, $P_{boil} = 0$ W, $Q_w = 0.06$ kg·s^{-1}, $\dot{m}^s_{air} = 0.03$ kg·s^{-1}, $Y_{wood} = 0.3$, $Y_{card} = 0.4$, $Y_{PVC} = 0.3$). Oxygen and temperature fields have been chosen for representation because of their importance in the incineration process. However, such results could have been drawn for any other chemical species.

As expected, oxygen mass fraction in the emulsion is zero (left side of the Figure 9) providing pyrolysis conditions for the initial waste conversion step and preventing the heterogeneous reaction from taking place in this part of the furnace. The oxidizing environment is encountered both in the buffer and disengagement zones. Oxygen concentration in the latter one is much more important than in the first one, which demonstrates the importance of the second fitting parameter (α). The concentration increases in the post combustion step because of the secondary air supply.

The temperature homogenization is well represented in the bed confirming the importance of sand in such a process. Maximum temperatures are obtained in the buffer and disengagement zones, which indicates the volatile and carbon particles combustion location. The cold secondary air supply explains the decrease of the temperature in the post combustion region. The zero value for the power evacuated by the in-bed boiler explains the high level of temperature encountered.

Influence of superficial velocity

In this paragraph every operating parameter is fixed ($T_{air} = 298$ K, $P_{boil} = 0$ W, $Q_w = 0.06$ kg·s^{-1}, $\dot{m}^s_{air} = 0$ kg·s^{-1}, $Y_{wood} = 0.3$, $Y_{card} = 0.4$, $Y_{PVC} = 0.3$), except for the superficial velocity which is varied in the range 1.3–2.5 m·s^{-1}. The rate is changed in steps of 0.1 m·s^{-1}.

First of all, as suggested by Figure 10, the whole superficial velocity range does not give acceptable solutions. Because the ratio γ defined (Eq. 54) and which represents the ratio of carbon particles to those of sand, is greater than 8%, the influence of reactive particles on hydrodynamical behavior of the bed cannot be neglected. This constitutes a lower limit for the superficial velocity.

$$\gamma = \frac{W_C}{A_c L_{mf} (1 - \epsilon_{mf}) \rho_{sand}} \tag{54}$$

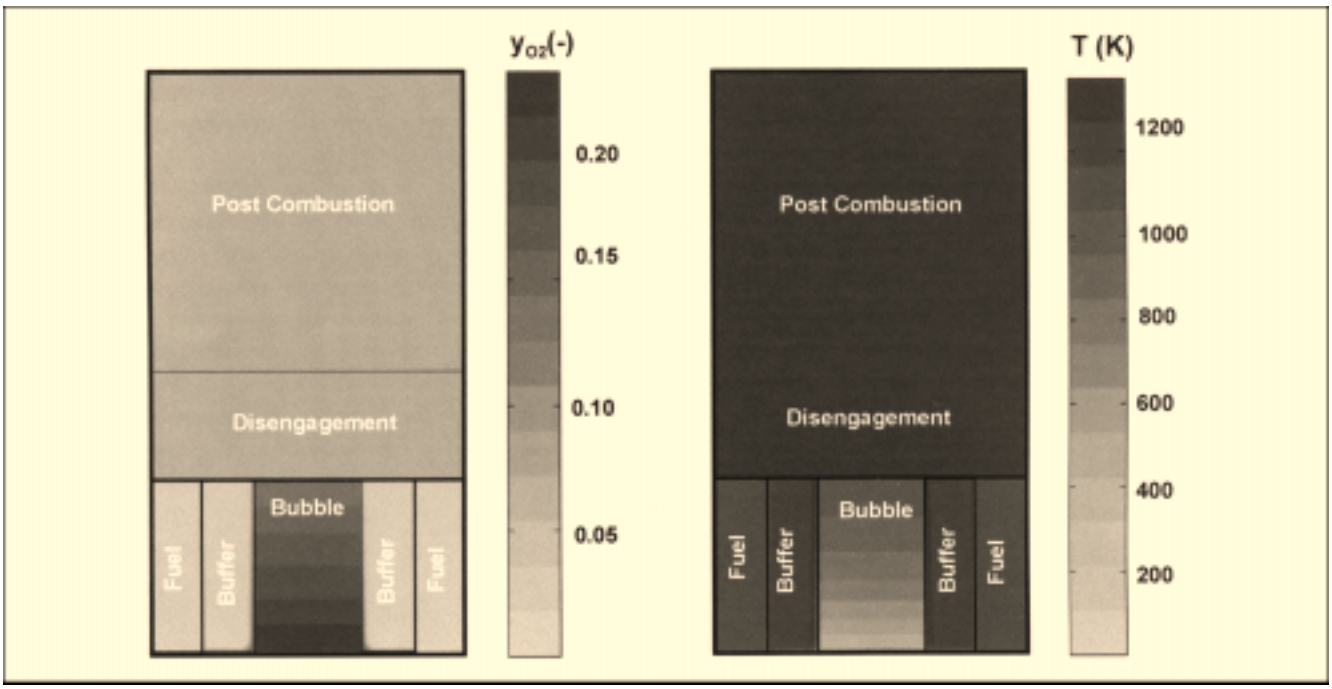

Figure 9. Overall model result for a set of given operating parameters.

Oxygen mass fraction (left) and temperature (right) fields.

When the superficial velocity is larger than 1.7 $m \cdot s^{-1}$, which is the lower validity limit, the carbon load decreases because the local oxygen concentration increases. This points out external diffusion control.

Figures 11 and 12 show the exhaust gas composition as a function of superficial velocity. First of all, as suggested by Figure 11 and the low level of carbon monoxide emissions encountered, a quasi complete oxidation of the pyrolyzed species may be achieved in the range of superficial velocity covered by the simulations. A simultaneous decrease of CO_2 and H_2O emissions and an increase in O_2 emissions (Figure 11) together with a bed temperature decrease (Figure 12) confirms this tendency. An excess of air, introduced as superficial velocity, increases the action of dilution for the chemical system.

The main influence of this increase is observed on pollutant emissions. For instance, the reduction of HCl emissions

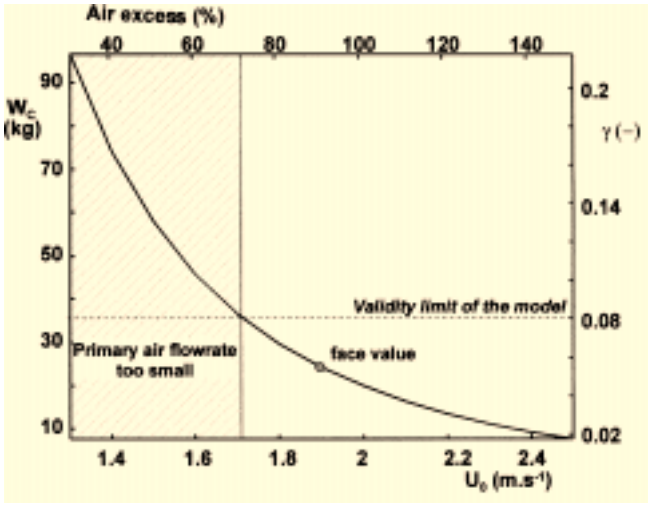

Figure 10. Influence of superficial velocity on carbon load in the bed for a set of given operating parameters.

$T_{air} = 298$ K, $P_{boil} = 0$W, $Q_W = 0.06$ kg·s^{-1}, $= 0$ kg·s^{-1}, $Y_{wood} = 0.3$, $Y_{card} = 0.4$, $Y_{PVC} = 0.3$).

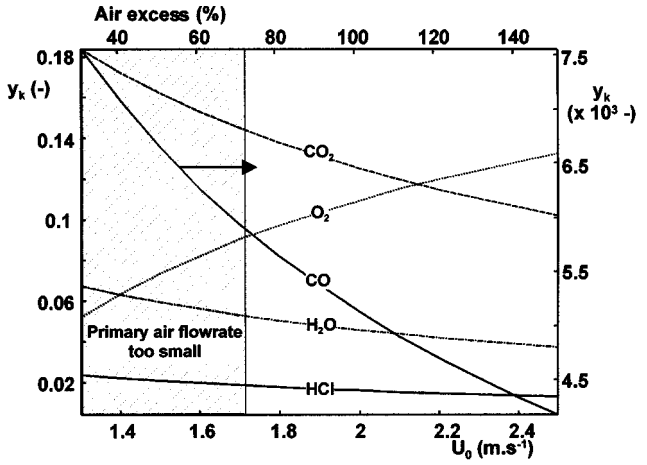

Figure 11. Influence of superficial velocity on gaseous stable product species mass fraction at the exhaust of the bed for a set of given operating parameters.

$T_{air} = 298$ K, $P_{boil} = 0$W, $Q_W = 0.06$ kg·s^{-1}, $= 0$ kg·s^{-1}, $Y_{wood} = 0.3$, $Y_{card} = 0.4$, $Y_{PVC} = 0.3$).

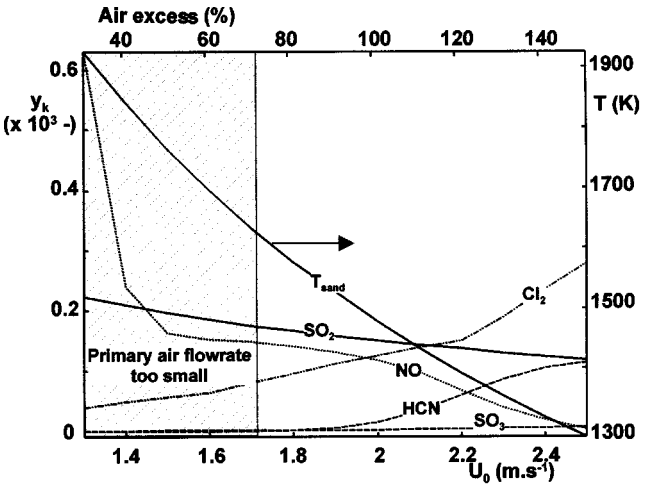

Figure 12. Influence of superficial velocity on gaseous pollutant species mass fraction at the exhaust of the bed and on temperature of the bed for a set of given operating parameters.

$T_{air} = 298$ K, $P_{boil} = 0$W, $Q_W = 0.06$ kg·s^{-1}, $= 0$ kg·s^{-1}, $Y_{wood} = 0.3$, $Y_{card} = 0.4$, $Y_{PVC} = 0.3$.

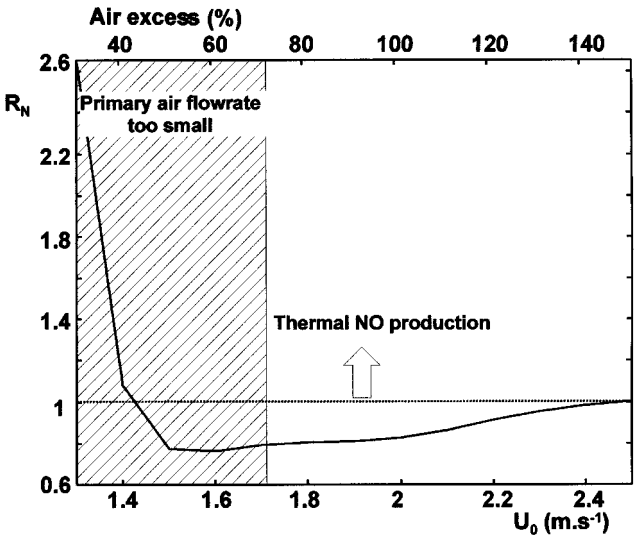

Figure 13. Influence of superficial velocity on ratio of NO_x to waste nitrogen content defined in Eq. 56 at the exhaust of the bed for a set of given operating parameters.

$T_{air} = 298$ K, $P_{boil} = 0$W, $Q_W = 0.06$ kg·s^{-1}, $= 0$ kg·s^{-1}, $Y_{wood} = 0.3$, $Y_{card} = 0.4$, $Y_{PVC} = 0.3$.

at the exhaust induces an increase in Cl_2 concentration. This modification in the chlorinated species concentrations is mainly due to the temperature decrease, promoting the reverse sense of Deacon's equilibrium

$$4HCl + O_2 \longleftrightarrow Cl_2 + 2H_2O \qquad (55)$$

In the same way, equilibrium between oxygen, sulfur dioxide, and sulfur trioxide (Eq. 44) promotes the formation of SO_3 as the temperature decreases. Nevertheless, its mass fraction remains small, and any further increase in superficial velocity should be used to raise sulfur trioxide mass fraction.

As the presence of excess air is very small, near the stoichiometry value, temperature is raised to 1,900 K. This high value promotes the activation of NO thermal mechanism, and Figure 13 gives further insight for this analysis. It represents the ratio of nitrogen contained in NO_x to nitrogen arising from waste pyrolysis R_N (Eq. 56).

$$R_N = \frac{\dot{m}_{HCN}^{exhaust}\dfrac{M_N}{M_{HCN}} + \dot{m}_{NO}^{exhaust}\dfrac{M_N}{M_{NO}}}{\dot{m}_{HCN}^{input}} \qquad (56)$$

The value of R_N, greater than one for rich conditions, points out the start of thermal NO mechanism. It indicates that nitrogen that does not arise from fuel is present in NO emissions. For this particular trend, only qualitative analysis can be drawn because of the high carbon load that exceeds the validity limit of the model.

If superficial velocity is larger than 1.5 m·s^{-1}, temperature is lower than 1,800 K. As a consequence, only the fuel NO mechanism is expected to contribute to NO formation. The decrease in the oxidation of hydrogen cyanide can be explained by the collapse of the thermal level and the lower value for the activation energy of the NO reduction (Table 3).

Influence of initial waste composition

This part of the study focuses on the impact of initial waste composition on the working of the incinerator. Other operating parameters have been fixed to an intermediate value ($U_0 = 1.9$ m·s^{-1}, $T_{air} = 298$ K, $P_{boil} = 0$ W, $Q_w = 0.06$ kg·s^{-1}, $\dot{m}_{air}^{s} = 0$ kg·s^{-1}) and simulations have been performed for 21 points equally spaced in the overall initial waste ternary diagram. Figures 14 and 15 summarize those simulations after double bi-cubic interpolation of the results.

The ''a'' diagram on the left top side of Figure 14 represents the overall excess air introduced in the bed given, a superficial velocity. It is another representation of the last diagram on the lower side of Figure 3b, which represents the overall mixture fraction at stoichiometric conditions. These figures indicate that incineration of cardboard requires less air than wood and less air than PVC, which is linked to the higher concentration of heavy hydrocarbons.

The evolution of bed temperature with respect to initial waste composition is represented in Figure 14b. First of all, due to the adiabatic assumption, the wide temperature range (1,100–1,900 K) covered by this graph does not always have physical sense. For instance, a temperature of 1,900 K would destroy the furnace, as the sand would melt. However unrealistic it may be, these simulations provide tools to design the in-bed boiler, and tools to understand pollutant formation. Heavy hydrocarbons (benzene in PVC) and lighter hydrocarbons (there being more methane in wood than in cardboard) are predicted for higher adiabatic temperatures.

Information concerning heterogeneous reaction (Eq. 10) can be found in Figure 14c. As fixed carbon wood content is more important than cardboard content, carbon load rises as

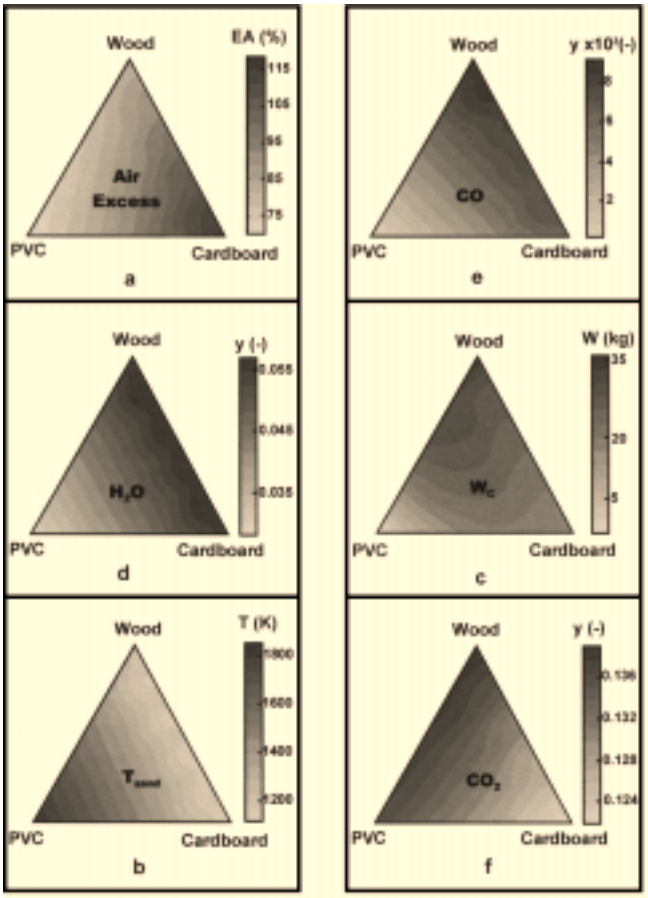

Figure 14. Influence of initial waste composition on data depicted on the figure for a set of given operating parameters.

$T_{air} = 298$ K, $U = 1.9$ m·s^{-1}, $P_{boil} = 0$W, $Q_W = 0.06$ kg·s^{-1}, $= 0$kg·s^{-1}.

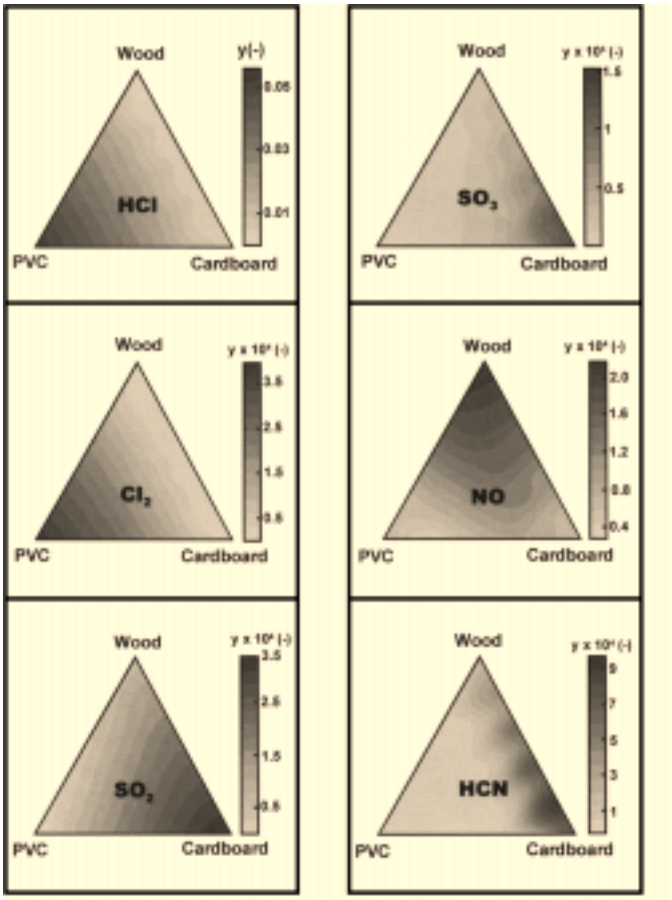

Figure 15. Influence of initial waste composition on data depicted on the figure for a set of given operating parameters.

$T_{air} = 298$, $U = 1.9$ m·s^{-1}, $P_{boil} = 0$W, $Q_W = 0.06$ kg·s^{-1}, $= 0$ kg·s^{-1}.

the fraction of wood in the initial waste increases. Because of the lower excess air on the wood-PVC binary side of the diagram, and due to the external diffusion control, carbon load is higher in this region. As expected, this load is zero when just PVC is incinerated.

The three diagrams of the lower part of this figure represent (Figures 14d–14f, respectively) water, carbon monoxide, and carbon dioxide mass fractions at the exhaust of the furnace. As previously exhibited, the working conditions of the furnace are acceptable since small quantities of carbon monoxide are emitted. The maximum emission of carbon monoxide, as well as carbon dioxide, is reached in the case of wood because of its high carbon content (Table 1). A low value of carbon dioxide mass fraction at the exhaust of the furnace is linked to dilution of the chemical system increasing overall excess air. Because of the moisture content of wood and cardboard, more water is exhausted on the wood-carbon binary side of the diagram.

Figure 15 provides evolution of pollutant emissions with respect to initial waste composition. Variations in the amount of chlorinated and sulfur-based pollutants are mainly due to their initial waste sulfur and chlorine content. Of course, similar trends can be drawn in the case of nitrogen base pollutants. Nevertheless, the mechanisms which produce NO_x are much more complex. For instance, the peak value of nitric oxide mass fraction is obtained in the case of wood because of its initial content. Sliding towards cardboard, on the binary line wood-cardboard, NO concentration in the exhaust gas diminishes softly, whereas the HCN concentration raises and exhibits a peak value in the case of cardboard. As waste is mainly composed of cardboard, the temperature in the post combustion zone ($\approx$1,100 K) does not allow for the fuel bound mechanism to be significantly engaged. This explains why the main part of the cardboard nitrogen content is exhausted as hydrogen cyanide.

Because of the nonzero value for NO emissions in the case of PVC, the important thermal level encountered for the burning of this material ($\approx$1,900 K) is expected to be sufficient for the thermal NO production mechanism to be engaged.

Influence of power evacuated by the in-bed boiler

In order to decrease the thermal level of the bed, an in-bed boiler is generally used to evacuate the power released by incineration. As shown in the previous paragraphs, adiabatic operation of the bed leads to a temperature which might de-

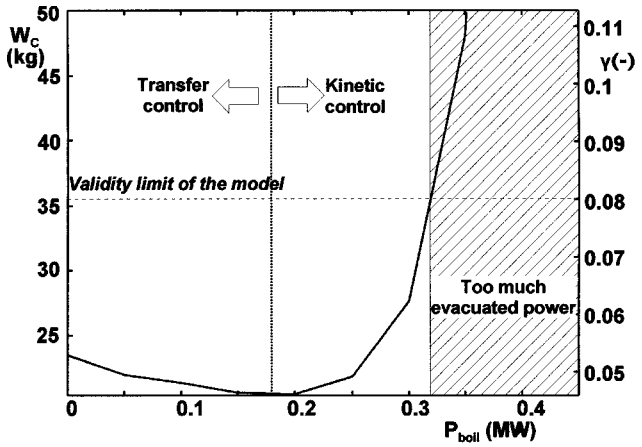

Figure 16. Influence of power evacuated by the in-bed boiler carbon load in the bed and air-flow rate crossing the buffer zone for a set of given operating parameters.

$T_{air} = 298$ K, $U = 1.9$ m·s^{-1}, $P_{boil} = 0$W, $Q_W = 0.06$ kg·s^{-1}, $= 0$, kg·s^{-1}, $Y_{wood} = 0.3$, $Y_{card} = 0.4$, $Y_{PVC} = 0.3$.

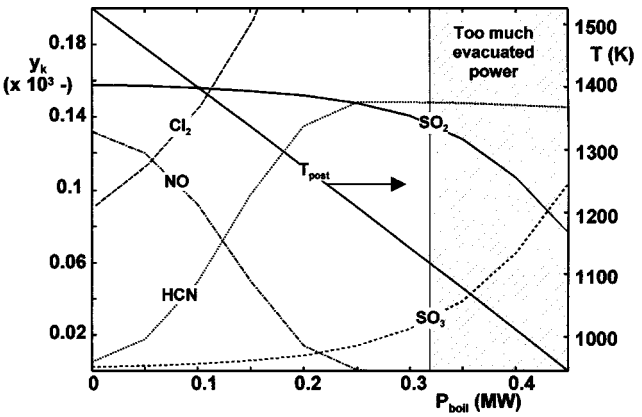

Figure 17. Influence of power evacuated by the in-bed boiler on pollutants mass fraction at the exhaust of the bed for a set of given operating parameters.

$T_{air} = 298$ K, $U = 1.9$ m·s^{-1}, $P_{boil} = 0$W, $Q_W = 0.06$ kg·s^{-1}, $= 0$ kg·s^{-1}, $Y_{wood} = 0.3$, $Y_{card} = 0.4$, $Y_{PVC} = 0.3$.

stroy the furnace. In this part of the study, the influence of the power removed by the boiler is evaluated through ten simulations. Given a set of other operating parameters ($U =$ 1.9 m·s^{-1} $T_{air} = 298$ K, $Qw = 0.06$ kg·s^{-1}, $\dot{m}^s_{air} = 0$ kg·s^{-1}, $Y_{wood} = 0.3$, $Y_{card} = 0.4$, $Y_{PVC} = 0.3$), P^{boil} is varied in the range 0−450 kW. Results of these simulations are provided in Figures 14 and 15.

Figure 16 shows the evolution of the carbon load in the bed with respect to the power evacuated by the in-bed boiler. Two separate behaviors are found. Actually, when the power evacuated is lower than 180 kW, the carbon load decreases as the power evacuated increases. This trend can be explained by the increase of the buffer zone width, linked to the decrease of the incipient fluidization velocity with temperature. As shown on Figure 17, the temperature of the bed always decreases. When the power evacuated by the boiler is greater than 180 kW, the increase in the carbon load is very important and is linked to the kinetic control of the heterogeneous reaction (Eq. 10). In order to respect the range of validity of the model, the power evacuated by the boiler should not exceed 300 kW.

Trends in the composition of the exhaust gas can be explained by the evolution of temperature, as has been done previously.

Results presented depict the influence of three operating parameters, namely superficial velocity, initial waste composition, and power evacuated by the in-bed boiler. The model gives insights into the influence of other operating parameters (secondary air-flow rate, temperature of the primary or secondary air, and waste flow rate), as well as geometrical settings (bed diameter, sand diameter...). Results of such simulations can be found elsewhere (Marias, 1999).

Conclusion

A model of a fluidized-bed incineration process has been developed. It takes into account most of the physico-chemical steps which may contribute to incineration in such a system. The wide variety of ordinary waste has been lumped into a simplified system composed of wood, cardboard, and PVC to represent plastics. Pyrolysis operation involved by introduction of this waste in the fluidized-bed furnace has been taken into account by the building of an equivalent input. It is composed of a high heating value gas, carbon particles of the same size distribution as the initial waste, gaseous atomic pollutants (nitrogen and sulfur) and ashes. Improvements of Werther's hydrodynamic model have been proposed in order to take into account volatile transfer from emulsion to bubbles. The building of a two-dimensional reactive zone, called the buffer zone, in place of Wether's film, is one of the main improvements. Transient balance equations for chemical species and total enthalpy have been given, as well as carbonaceous particles population balance. Finally, the proposed approach is a two free parameter model, which should be used in simulation or control strategies.

Resolving of the overall model has been performed in three successive steps using a superimposition technique. Chemical and temperature fields inherent in volatile combustion have been computed using the mixture fraction concept. Variations in those fields due to carbon heterogeneous combustion, computed in the second step, are superimposed onto these previous fields. Then, in a third step, pollutants, namely NO_x and SO_x emissions, are computed in a post processing stage. Kinetic rates have been used to describe both thermal and fuel-bound NO_x formation, and chemical equilibrium has been assumed to be reached for the evaluation of SO_x production.

Steady-state operation simulations have been performed in order to describe the influence of three operating parameters (superficial velocity, initial waste composition and power evacuated by the in-bed boiler) on the furnace exhaust. A good qualitative agreement is given by the model. Nevertheless, experimental data would be useful in order to fix the value of the two relevant parameters used by the model. On this basis, the model should provide good quantitative agreement with these data. By construction, the model is highly

evolutionary, and, for instance, sub-models relative to other pollutants could easily be implemented.

This model is the first step in an overall project of building a real-time simulator of a whole incineration process which should include dust removal, scrubbing, and so on. To achieve the goal, the first objective must be to drastically reduce the computer processing time required by transient simulations. This reduction has been performed in steady-state simulation using neural networks, and this technique is expected to be used again to reach our goal.

Notation

a = specific area of the bed (Werther, 1980) (m^{-1})
A_c = cross-sectional surface of the bed (m^2)
A_{ech} = total exchange area in the bed (m^2)
Ar = Archimede's number
Ash = ash content (%)
c_{p_i} = constant pressure specific heat of i ($J \cdot kg^{-1} \cdot K^{-1}$)
C_{fixed} = fixed carbon content (%)
d = particle diameter (m)
D = diffusion coefficient ($m^2 \cdot s^{-1}$)
F_0 = mass flow rate of carbon particle in the equivalent input ($kg \cdot s^{-1}$)
F_1 = mass flow rate in the carry over ($kg \cdot s^{-1}$)
F_2 = mass flow rate elutriated ($kg \cdot s^{-1}$)
g = gravity acceleration ($m \cdot s^{-2}$)
f = mixture fraction
F_w = mass flow rate of sand entrained in the disengaging zone ($kg \cdot s^{-1}$)
h = heat exchange coefficient ($W \cdot m^{-2}$)
$h^0_{f,i}$ = standard enthalpy of formation of i ($J \cdot kg^{-1}$)
H = total enthalpy (1) ($J \cdot kg^{-1}$)
k_m = external transfer coefficient for heterogeneous reaction (10) ($m \cdot s^{-1}$)
k_s = kinetic constant of heterogeneous reaction (10) ($m \cdot s^{-1}$)
L^{bed} = expanded bed height (m)
L^{dis} = disengaging zone height (m)
L_v = latent heat of water vaporization ($J \cdot kg^{-1}$)
$\dot{m}$ = mass flow rate ($kg \cdot s^{-1}$)
M = molar weight ($kg \cdot mol^{-1}$)
$n(r)$ = density number of particles which radius is included in $[r, r + dr]$
N = nitrogen content (%) or total number of gaseous species
Nu = Nusselt number
P = power (W)
P_{atm} = atomspheric pressure (Pa)
$Q_{\dot{w}}$ = initial waste flow rate ($kg \cdot s^{-1}$)
$\dot{Q}$ = total enthalpy source term ($W \cdot m^{-3}$)
r = carbon particle radius (m)
R = chemical reaction rate ($kg \cdot m^{-3} \cdot s^{-1}$) or ideal gas constant ($J \cdot mol^{-1} \cdot K^{-1}$)
Re_{mf} = Reynolds number at incipient fluidization (Prins, 1987)
$\bar{R}_s$ = average specific reaction rate for a carbon particle inside the bed ($kg \cdot m^{-2} \cdot s^{-1}$)
S = sulphur content (%)
Sc = Schmidt number
S_{reac} = surface offered by a carbon particle to reaction in the (m^2)
T = absolute temperature (K)
T_{ref} = reference temperature (298 K)
U = fluidization velocity ($m \cdot s^{-1}$)
$U(z)$ = superficial velocity inside bubble zone ($m \cdot s^{-1}$)
U_1 = equivalent fluidization velocity (Eq. 2) ($m \cdot s^{-1}$)
U_{mf} = incipient fluidization velocity ($m \cdot s^{-1}$)
U_t = terminal velocity of particles ($m \cdot s^{-1}$)
Vol = volatile constant (%)
W = mass (kg)
x = molar fraction
y = mass fraction or transversal space co-ordinate in the buffer zone (m)
Y = mass fraction in the initial waste
z = height above the distributor (m)

Greek letters

α = ratio of mass of carbon in the disengaging zone to bed one (Eq. 53)
β = ratio of carbon molar weight to oxygen one
δ = buffer zone thickness (Eq. 52) (m)
$\Delta_r H$ = enthalpy of reaction ($J \cdot kg^{-1}$)
ϵ_b = volume fraction of the bed occupied by bubbles (Werther, 1980)
ϵ_d = porosity in the disengaging zone
ϵ_{mf} = porosity at incipient fluidization
Λ = stoichiometry coefficient (10)
μ = dynamic viscosity ($Pa \cdot s$)
ρ = density ($kg \cdot m^{-3}$)
$\rho^{dis}_{O_2}$ = mass concentration of oxygen in the disengaging zone ($kg \cdot m^{-3}$)
τ = residence time of sand particles in the disengaging zone (s)
ϕ = carbon particle size distribution in the furnace
ϕ_0 = initial waste particle-size distribution
φ_{vol} = specific mass flow rate of volatile from emulsion to bubbles ($kg \cdot m^{-2} \cdot s^{-1}$)
ω = rate of shrinkage of carbon particles ($m \cdot s^{-1}$)

Subscripts

air = relative to fluidization air
boil = relative to in-bed boiler
C = relative to carbon particles
dry = relative to initial waste drying
emul = relative to emulsion zone
fuel = relative to fuel-bound NO mechanism formation
pyro = relative to initial waste pyrolysis
sand = relative to sand
thermal = relative to thermal NO mechanism formation
vol = relative to initial waste volatile content

Superscripts

bubble = relative to bubble zone
buff = relative to buffer zone
card = relative to cardboard
dis = relative to disengaging zone
emul = relative to emulsion zone
partic = realative to carbon particles
post = relative to post combustion zone
PVC = relative to polyvinyl chloride
sand = relative to sand
sec = relative to secondary air flow rate
wood = relative to wood

Literature Cited

Adanez, J., and J. C. Abanades, "Modeling of Lignite Combustion in Atmospheric Fluidized Bed Combustors. 1 Selection of Submodels and Sensitivity Analysis," *Ind. Eng. Chem. Res.*, **31**, 2286 (1992).

Adanez, J., and J. C. Abanades, "Modeling of Lignite Combustion in Atmospheric Fluidized Bed Combustors. 2 Model Validation and Simulation," *Ind. Eng. Chem. Res.*, **31**, 2296 (1992).

Ademe, "Atlas Professionnel des Déchets en France," CD-Rom (1998).

Agarwal, P. K., and A. K. Wildegger-Gaissmaier, "Combustion of Coal Volatiles in Gas Fluidized Beds," *Chem. Eng. Res. Des.*, **64**, 431 (1987).

Avedesian, M. M., and J. F. Davidson, "Combustion of Carbon Particles in a Fluidized Bed," *Trans. Inst. Chem. Eng.*, **51**, 121 (1973).

Baker, R. R., "Thermal Decomposition of Cellulose," *J. of Thermal Analysis*, **8**, 163 (1975).

Beck, S. R., and M. J. Wang, "Wood Gasification in a Fluidized Bed," *Ind. Eng. Chem Process Des. Dev.*, **19**, 312 (1980).

Bilodeau, J. F., N. Thérien, P. Proulx, S. Czernick, and E. Chornet, "A Mathematical Model of Fluidized Bed Biomass Gasification," *Can. J. Chem. Eng.*, **71**, 549 (1993).

Bockhorn, H., A. Hornung, U. Hornung, S. Teepe, and J. Weichmann, "Investigation of the Kinetics of Thermal Degradation of Commodity Plastics," *Combust. Sci. Tech.*, **116-117**, 129 (1996).

Borghi, R., and M. Destriau, *La Combustion et les Flammes*, Editions Technip, Paris (1995).
Brem, G., ''Mathematical Modeling of Coal Conversion Processes with Application to Atmospheric Fluidized Bed Combustion,'' PhD Thesis, TNO Netherlands Organization for Applied Scientific Research (1990).
Bukur, D., and R. Amundson, ''Mathematical Modelling of Fluidized Bed Reactors: III. Axial Dispersion Model,'' *Chem. Eng. Sci.*, **30**, 1159 (1975).
Caubet, S., P. Corte, C. Fahim, and J. P. Traverse, ''Thermochemical Conversion of Biomass: Gasification by Flash Pyrolysis Study,'' *Solar Energy*, **29**, 565 (1982).
Chigier, N., *Energy Combustion and Environment*, McGraw-Hill, New York (1981).
Clough, S. J., and J. F. Stubington, ''The Transition from Laminar to Turbulent Flow in the Dense Phase of a Fluidized Bed and Its Effect on Mass Transfer, Heat Transfer and Particle Classification Boundaries,'' *Fluidization VIII*, Tours, France, *Engineering Foundation*, New York, 271, (May 14–19, 1995).
Davidson, J. F., and D. Harrison, *Fluidized Particles*, Cambridge Univ. Press, New York (1963).
Deglise, X., and J. Lede, ''Valorisation par Voie Thermique de la Biomasse,'' *Entropie*, **94**, 24 (1980).
Delbourgo, R., and H. Mellotée, ''Combustion,'' Les Techniques de l'Ingénieur, A3170 (1983).
De Soete, G. G., ''Overall Reaction Rates of NO and N_2 Formation from Fuel Nitrogen,'' *15th Symp. (Int'l.) on Combustion. The Combustion Institute*, 1093 (1975).
De Souza-Santos, M. L., ''Comprehensive Modelling and Simulation of Fluidized Bed Boilers and Gasifiers,'' *Fuel*, **68**, 1507 (1989).
Dif, B., ''Pyrolyse-Gazéification de la Biomasse. *Conception et Mise au Point d'un Réacteur à Lit Fluidisé*,'' Thèse de l'Institut National Polytechnique de Lorraine (1987).
Doraiswamy, L. K., and M. M. Sharma, ''Heterogeneous Reactions: Analysis, Examples, and Reactor Design: 1. Gas-Solid and Solid-Solid Reactions,'' Wiley Interscience, New York (1984).
El Ghezal, L., ''Contribution à l'Étude de la Pyrolyse Rapide et de la Vapogazeification de Sciure de Bois dans un Réacteur à Lit Fluidisé de Sable Chaud,'' Thèse de l'Institut National Polytechnique de Toulouse, France (1983).
El Mezni, T., ''Contribution à l'Étude d'un lit Fluidisé Turbulent en Combustion,'' Thèse, Ecole Nationale Supérieure des Mines de Paris, France (1985).
Fluent 5 User's Guide (1998).
Glassman, I., *Combustion, Third Edition*, Academic Press, San Diego (1996).
Graham, R. G., and M. A. Bergougnou, ''Fast Pyrolysis of Biomass,'' *J. Analyt. Appl. Pyr.*, **6**, 95 (1984).
Gordon, A. L., and N. R. Amundson, ''Modeling of Fluidized Bed Reactors: IV. Combustion of Carbon Particles,'' *Chem. Eng. Sci.*, **31**, 1163 (1976).
Hannes, J., ''Mathematical Modelling of Circulating Fluidized Bed Combustion,'' PhD Thesis, T.U. Delft, The Netherlands (1996).
Hemati, M., ''Etude de la Pyrolyse et de la Gazéification de Bois par Thermogravimétrie et en Lit Fluidisé de Catalyseur,'' Thése, Institut National Polytechnique de Toulouse, France (1984).
Ishida, M., and Y. Wen, ''Comparison of Kinetic and Diffusional Models for Solid-Gas Reactions,'' *AIChE J.*, **14**, 311 (1968).
Ishida, M., and Y. Wen, ''Comparison of Zone Reaction Model and Unreacted-Core Shrinking Model Solid-Gas Reactions: I. Isothermal Analysis,'' *Chem. Eng. Sci.*, **26**, 1031 (1971).
Ishida, M., and Y. Wen, ''Comparison of Zone Reaction Model and Unreacted-Core Shrinking Model in Solid-Gas Reactions: II. Non-Isothermal Analysis,'' *Chem. Eng. Sci.*, **26**, 1043 (1971).
Junk, K. W., and R. C. Brown, ''A Model of Coal Combustion Dynamics in a Fluidized Bed Combustor,'' *Combustion and Flame*, **95**, 219 (1993).
Kashiwagi, T., and H. Nambu, ''Global Kinetic Constants for Thermal Oxidative Degradation of a Cellulosic Paper,'' *Combustion and Flame*, **88**, 345 (1992).
Kato, K., and C. Y. Wen, ''Bubble Assemblage Model for Fluidized Bed Catalytic Reactors,'' *Chem. Eng. Sci.*, **24**, 1351 (1969).
Kung, H. C., and A. S. Kalelkar, ''On the Heat of Reaction in Wood Pyrolysis,'' *Combustion and Flame*, **20**, 91 (1973).
Kunii, D., and O. Levenspiel, *Fluidization Engineering*, second edition, Butterworth-Heinemann Series in Chemical Engineering, Boston (1991).
Kuo, K. K., *Principles of Combustion*, Wiley-Interscience, New York (1986).
Lee, D. C., J. L. Hodges, and C. Georgakis, ''Modelling SO_2 Emissions from Fluidized Bed Coal Combustors,'' *Chem. Eng. Science*, **35**, 302 (1980).
La Nauze, R. D., ''Fundamentals of Coal Combustion in Fluidized Beds,'' *Chem. Eng. Res. Des.*, **63**, 3 (1985).
Marias, F., ''Procédé d'incinération d'un Déchet Modèle: de l'approche Physique aux Simulations en Lit Fluidisé,'' Thèse, Universite de Pau et des Pays de l'Adour, France (1984).
Matlab, Neural Network Toolbox User's guide (1998).
Milioli, F. E., and P. J. Foster, ''Entrainment and Elutriation Modelling in Bubbling Fluidized Beds,'' *Powder Technol.*, **83**, 223 (1995).
Ogada, T., and J. Werther, ''Combustion Characteristics of Wet Sludge in a Fluidized Bed,'' *Fuel*, **75**, 617 (1996).
Paladino, O., S. Zucotti, P. Costa, and P. Fontana, ''A Semi-Dynamic Model of a Fluidized-Bed Waste Combustor,'' *Chem. Biochem. Eng.*, **6**, 617 (1992).
Park, D., O. Levenspiel, and T. J. Fitzgerald, ''A Comparison of the Plume Model with Currently used Models for Atmospheric Fluidized Bed Combustion,'' *Chem. Eng. Sci.*, **35**, 295 (1980).
Preto, F., ''Studies and Modelling of Atmospheric Fluidized Bed Combustion of Coal,'' PhD Thesis, Queen's University at Kingston, (1987).
Prins, W., ''Fluidized Bed Combustion of a Single Carbon Particle,'' PhD Thesis, University of Twente (1987).
Robert, F., ''Bois Énergie,'' Les techniques de l'ingénieur, B1 I, A1705 (1989).
Roberts, A. F., ''A Review of Kinetics for the Pyrolysis of Wood and Related Substances,'' *Combustion and Flame*, **14**, 261 (1970).
Ross, I. B., and J. F. Davidson, ''The Combustion of Carbon Particles in a Fluidized Bed,'' *Trans. Inst. Chem. Eng.*, **59**, 108 (1981).
Ross, I. B., M. S. Patel, and J. F. Davidson, ''The Temperature of Burning Carbon Particles in Fluidized Beds,'' *Trans. Inst. Chem. Eng.*, **59**, 83 (1981).
Selçuk, N., O. Oymak, and E. Degirmenci, ''Basic Requirement for Modeling Fluidized Beds: Fast Computation of Particle Size Distribution (PSDs),'' *Powder Technol.*, **87**, 269 (1996).
Shafizadeh, F., ''Introduction to Pyrolysis of Biomass,'' *J. Analyt. App. Pyr.*, **3**, 283 (1982).
Sriramulu, S., S. Sane, P. Agarwal, and T. Mathews, ''Mathematical Modelling of Fluidized Bed Combustion: 1. Combustion of Carbon in Bubbling Beds,'' *Fuel*, **75**, 1351 (1996).
Stannmore, B. R., and K. Jung, ''The Burnout Rates of Brown Coal Char Particles in Fluidized Bed Combustors,'' *Trans. Inst. Chem. Eng.*, **58**, 66 (1980).
Stubington, J. F., and J. F. Davidson, ''Gas-Phase Combustion in Fluidized Bed, *AIChE J.*, **27**, 59 (1981).
Stubington, J. F., and S. W. Chan, ''On the Phase Location and Rate of Volatiles Combustion in Bubbling Fluidized Bed Combustors,'' *Trans. Inst. Chem. Eng.*, **68**, 195 (1990).
Stubington, J. F., and S. W. Chan, ''The Multiple Discrete Diffusion Flame Model for Fluidized Bed Combustion of Volatiles,'' 12th Intl. FBC Conf., ASME, New York, Vol. 1, 167 (1993).
Turnbull, E., and J. F. Davidson, ''Fluidized Combustion of Char and Volatiles from Coal,'' *AIChE J.*, **30**, 881 (1984).
Turnbull, E., E. R. Kossakowski, J. F. Davidson, R. B. Hopes, H. W. Blackshaw, and P. T. Y. Goodyer, ''Effect of Pressure on Combustion of Char in Fluidized Beds,'' *Chem. Eng. Res. Des.*, **62**, 223 (1984).
Turns, S. R., *An Introduction to Combustion*, McGraw-Hill, New York (1996).
Vovelle, C., and J. L. Delfau, ''Combustion des Plastiques,'' *Les Techniques de l'Ingénieur*, AM 3170 (1997).
Wen, C. Y., and R. F. Hashinger, ''Elutriation of Solid Particles from a Dense-Phase Fluidized Bed,'' *AIChE J.*, **6**, 220 (1960).
Werther, J., ''Modeling and Scale-Up of Industrial Fluidized Bed Reactors,'' *Chem. Eng. Sci.*, **35**, 372 (1980).
Wildegger-Gaissmaier, A. E., and P. K. Agarwal, ''Drying and Devolatilization of Large Coal Particles under Pyrolysis Conditions,'' *Trans. Inst. Chem. Eng.*, **68**, 251 (1990).

Zhou, X., ''Contribution à l'étude de l'incinération des Déchets Urbains: Expérimentation en Réacteur à Lit Fixe à contre courant, Approche Théorique du Déplacement du Front d'inflammation,'' Thèse de l'Université de Poitiers, France (1994).

Appendix: Other Balance Equations

Bubble zone

Balance Equation. Let us consider a control volume $A_c \times \epsilon_b \times dz$ of this zone.

Superficial velocity within this control volume is increased under the mass-flow rate of volatile from emulsion to bubble. A global mass balance leads to

$$U(z) = U_1 - U_{mf}(T_{\text{emul}}) + \frac{a\varphi_{\text{vol}} z}{\rho_{\text{emul}}}$$

Four contributions might modify the rate of accumulation of a chemical species in this volume (axial diffusion is neglected):

- The net transport of that species with ascending bubbles

$$\rho_{\text{emul}} A_c \left[U(z) y_k^{\text{bubble}}(z) - U(z+dz) y_k^{\text{bubble}}(z+dz) \right]$$

- The transport of that species with convective flow of volatile from emulsion at the boundary of the control volume: $\varphi_{\text{vol}} \text{adz}(y_k^{\text{buff}}|_{z,\ y=0})$
- The transport of that species with diffusion at the boundary of the volume:

$$-\rho_{\text{emul}} D a dz \left(-\left. \frac{\partial y_k^{\text{buff}}}{\partial y} \right|_{z,y=0} \right)$$

- The net chemical reaction rate of that specie: $\epsilon_b A_c dz R_k^{\text{bubble}}$

Given the rate of accumulation of that specie in the control volume $A_c dz(\partial \epsilon_b \rho_{\text{emul}} y_k^{\text{bubble}}/\partial t)$ the following balance equation is derived

$$\frac{\partial \epsilon_b \rho_{\text{emul}} y_k^{\text{bubble}}}{\partial t} = -\rho_{\text{emul}} \left[y_k^{\text{bubble}} \frac{\partial U}{\partial z} + U \frac{\partial y_k^{\text{bubble}}}{\partial z} \right] + \varphi_{\text{vol}} a y_k^{\text{buff}}|_{z,y=0} + \rho_{\text{emul}} a D \left. \frac{\partial y_k^{\text{buff}}}{\partial y} \right|_{z,y=0} + \epsilon_b R_{y_k}^{\text{bubble}}$$

Of course, the same formalism could be applied to total enthalpy and would lead to an equivalent equation.

Chemical Reaction Rate. This region is free of solid. Thus, only volatile combustion and pollutant formation may affect chemical reaction rate within this zone. As explained in the paragraph devoted to chemical reaction rate in the buffer zone, chemical equilibrium is supposed to be reached during volatile combustion. Thus, chemical reaction rates are evaluated through equilibrium tables (see the subsection on chemical reaction rate). Dealing with pollutant formation, the assumption used in the buffer zone prevails.

Volumetric Heat Generation. Because of the choice of total enthalpy to represent the energetic level of the system, because of the lack of solid particles within this zone, and because impact of pollutant formation on energetic level is neglected, the volumetric heat generation is zero

$$R_H^{\text{bubble}} = 0$$

Boundary Conditions. Continuity of fields of chemical species and total enthalpy from one zone to another implies

$$y_k^{\text{bubble}}(z=0,t) = y_k^{\text{air}}(t); \quad H^{\text{bubble}}(z=0,t) = H^{\text{air}}(t)$$

Moreover, at the outlet of the domain, it is supposed that there are no gradients in the axial direction

$$\left. \frac{\partial y_k^{\text{bubble}}}{\partial z} \right|_{z=L^{\text{bed}}} = 0; \quad \left. \frac{\partial H^{\text{bubble}}}{\partial z} \right|_{z=L^{\text{bed}}} = 0;$$

The emulsion

Balance Equation. Let us consider the total amount of gas $A_c L^{\text{bed}}(1\epsilon_b - a\delta)\epsilon_{mf}$ of the emulsion.

Six contributions might modify the rate of accumulation of a chemical species in this zone:

- The supply of fluidizing air: $\rho_{\text{emul}} A_c(1-a\delta) U_{mf} y_k^{\text{air}}$
- The outflow of this quantity leaving the emulsion: $\rho_{\text{emul}} A_c(1-a\delta) U_{\text{mf}} y_k^{\text{emul}}$
- The supply of the volatile matter: $\dot{m}_{\text{vol}} y_k^{\text{vol}}$
- Its outflow from the emulsion: $\dot{m}_{\text{vol}} y_k^{\text{emul}}$
- The transport of that species with diffusion at the boundary of the volume

$$-\rho_{\text{emul}} D \iint_{A_{ech}} \left. \frac{\partial y_k^{\text{buff}}}{\partial y} \right|_{y=\delta} dA$$

- The net chemical reaction rate of that species: $A_c L^{\text{bed}}(1 - \epsilon_b - a\delta)\epsilon_{\text{mf}} R_k^{\text{emul}}$.

Given the rate of accumulation of that species in the control volume $A_c \epsilon_{\text{mf}} [\partial \rho_{\text{emul}}(1-\epsilon_b - a\delta) L^{\text{bed}} y_k^{\text{emul}}/\partial t]$, the following balance equation is derived

$$A_c \epsilon_{mf} \frac{\partial \rho_{\text{emul}}(1-\epsilon_b - a\delta) L^{\text{bed}} y_k^{\text{emul}}}{\partial t} = \rho_{\text{emul}} A_c U_{mf} \left[y_k^{\text{air}} - y_k^{\text{emul}} \right] + \dot{m}_{\text{vol}} \left[y_k^{\text{vol}} - y_k^{\text{emul}} \right] - \rho_{\text{emul}} D \iint_{A_{ech}} \left. \frac{\partial y_k^{\text{buff}}}{\partial y} \right|_{y=\delta} dA + A_c L^{\text{bed}}(1-\epsilon_b - a\delta)\epsilon_{mf} R_k^{\text{emul}}$$

Once again, a similar formalism would lead to an equivalent equation for total enthalpy.

Chemical Reaction Rate. The combustion of volatile is expected to be much more rapid than the carbon particle one. That is why, we assume the oxygen present in this zone to be wholly consumed by volatile. Because of the choice of the heterogeneous reaction (Eq. 10), this assumption results in a lack of transformation of the fixed carbon within the emulsion.

As explained in the previous paragraphs, for volatile combustion, chemical reaction rates are evaluated through equilibrium tables, and, once again, we used the assumption formulated in the buffer zone for pollutant formation.

Volumetric Heat Generation. The previous paragraph has emphasized the lack of solid carbon oxidation within the emulsion. Thus, heat may be added or removed from this zone either by the heat transfer with solid particles, or either by the in-bed boiler. The total amount of heat removed by this one is referred to P_{boil}. The subsequent volumetric quantity is then

$$R_H^{\text{emul,boil}} = \frac{P\text{boil}}{A_c L^{\text{bed}}(1-\epsilon_b - a\delta)\epsilon_{mf}}$$

Assuming equiprobability of presence of sand particles (held in the bubbling bed) within the buffer-emulsion system, one is able to estimate the area offered to convective heat transfer within the control volume

$$S^{\text{emul,sand}} = \frac{6\left(W_{\text{sand}} - W_{\text{sand}}^{\text{dis}}\right)}{\rho_{\text{sand}} d_{\text{sand}}} \frac{(1-\epsilon_b - a\delta)}{(1-\epsilon_b)}$$

The subsequent amount of heat transferred is then

$$P^{\text{emul, sand}} = \frac{6\left(W_{\text{sand}} - W_{\text{sand}}^{\text{dis}}\right)}{\rho_{\text{sand}} d_{\text{sand}}} \frac{(1-\epsilon_b - a\delta)}{(1-\epsilon_b)} h\left(T^{\text{sand}} - T^{\text{emul}}\right)$$

and the volumetric heat generation required in the total enthalpy balance equation becomes

$$R_H^{\text{emul,sand}} = \frac{6\left(W_{\text{sand}} - W_{\text{sand}}^{\text{dis}}\right)}{\rho_{\text{sand}} d_{\text{sand}}(1-\epsilon_b) A_C L^{\text{bed}} \epsilon_{mf}} h\left(T^{\text{sand}} - T^{\text{emul}}\right)$$

Heat transfer with char particles is taken into account using the same formalism as in the case of the buffer zone

$$R_H^{\text{emul,partic}} = (1-\alpha)\frac{3W_C}{\rho_C A_C L^{\text{bed}} \epsilon_{mf}(1-\epsilon_b)} \int_0^{R_m} \frac{h(r)\left(T_C(r) - T^{\text{emul}}\right)\phi(r)}{r} dr$$

Of course, $R_H^{\text{emul}} = R_H^{\text{emul,boil}} + R_H^{\text{emul, sand}} + R_H^{\text{emul,part}}$

The disengagement zone

Balance Equation. Let us consider the total amount of gas $A_C L^{\text{dis}} \epsilon_d$ of the disengagement zone.

Five contributions might modify the rate of accumulation of a chemical species in this zone:

- The gas entering this zone from the bubble one: $\rho_{\text{emul}} A_c U(L^{\text{bed}}) y_k^{\text{bubble}}(L^{\text{bed}})$
- The gas entering this zone from the buffer one: $a\rho_{\text{emul}} A_c U_{\text{mf}} \int_0^{\delta} y_k^{\text{buff}}(y, L^{\text{bed}}) dy$
- The gas entering this zone from the emulsion: $\rho_{\text{emul}} A_c (1 - a\delta) U_{\text{mf}} y_k^{\text{emul}}$
- The gas leaving this zone to the post-combustion one $\rho_{\text{emul}} A_c [(U(L^{\text{bed}}) + U_{\text{mf}}] y_k^{\text{dis}}$
- The net chemical reaction rate of that species: $\epsilon_d A_c L^{\text{dis}} R_k^{\text{dis}}$

Given the rate of accumulation of that species in the control volume $A_c[(\partial \epsilon_d \rho_{\text{emul}} L^{\text{dis}} y_k^{\text{dis}})/\partial t]$ the following balance equation is derived

$$A_c \frac{\partial \epsilon_d \rho_{\text{emul}} L^{\text{dis}} y_k^{\text{dis}}}{\partial t} = \rho_{\text{emul}} U(L^{\text{bed}}) y_k^{\text{bubble}}(L^{\text{bed}}) + a\rho_{\text{emul}} U_{mf} \int_0^{\delta} y_k^{\text{buff}}(y, L^{\text{bed}}) + (1-a\delta)\rho_{\text{emul}} U_m y_k^{\text{emul}} - \rho_{\text{emul}}\left[U(L^{\text{bed}}) + U_{mf}\right] y_k^{\text{dis}} + \epsilon_d A_c L^{\text{dis}} R_k^{\text{dis}}$$

Chemical Reaction Rate. As in the buffer zone, both volatile and char combustion may coexist within the disengagement. Using the same assumption, the chemical reaction rate due to volatile combustion is evaluated through equilibrium tables.

Given the size distribution $\phi(r)$ of the carbon pellets inside the bed, the number of these pellets of which the radius is between r and $r + dr$ and present in the disengagement is

$$N^{\text{dis}}(r) = \alpha \frac{3W_C \phi(r) dr}{4\pi\rho_C r^3}$$

The computation of the area involved by the reaction inside this zone can easily be derived

$$S^{\text{dis,partic}}(r) = \alpha \frac{3W_C \phi(r) dr}{r\rho_C}$$

Because the reaction is expected to take place at the external surface of the particle, and because it is supposed to be both kinetic and external transfer limited, the chemical reaction rate can now be processed (in the case of oxygen), once all the radii of particles have been included

$$R_{O_2}^{\text{dis,partic}} = -\alpha \frac{3W_C M_{O_2}[O_2]^{\text{dis}}}{\rho_c A_c L^{\text{dis}} \epsilon_d} \int_0^{R_m} \frac{\Lambda k_m(r) k_s(r) \phi(r)}{\left[\Lambda k_s(r) + k_m(r)\right] r} dr$$

Corresponding chemical reaction rates for carbon monoxide and dioxide are obtained using the stoichiometry of reaction (Eq. 10).

As has already been assumed, pollutant formation only affects chemical reaction rate, and is computed as described earlier.

Volumetric Heat Generation. The assumptions used in the buffer zone are also applied in the disengagement. The contribution of reacting particles to the heat generated in this region is translated from the buffer one

$$R_H^{\text{dis,part}} = \frac{\beta}{\Lambda} R_{O_2}^{\text{dis,part}} h_{f,C}^0 + \alpha \frac{3W_C}{\rho_C A_C L^{\text{dis}} \epsilon_d} \int_0^{R_m} \frac{h(r)\left[T_C(r) - T^{\text{dis}}\right]\phi(r)}{r} dr$$

Such a translation may also be applied to the volumetric heat generation due to heat transfer with sand particles

$$S^{\text{dis,sand}} = \frac{6W^{\text{dis}}_{\text{sand}}}{\rho_{\text{sand}} d_{\text{sand}}}$$

Then, the volumetric heat generation due to sand can easily be derived

$$R_H^{\text{dis,sand}} = \frac{6W^{\text{dis}}_{\text{sand}}}{\rho_{\text{sand}} d_{\text{sand}} A_c L^{\text{dis}} \epsilon_d} h\left(T^{\text{sand}} - T^{\text{dis}}\right)$$

The total heat released within the disengagement is the sum of the two previous ones

$$R_H^{\text{dis}} = R_H^{\text{dis,part}} + R_H^{\text{dis,sand}}$$

Post-combustion zone

Balance Equation. Let us consider the total amount of gas $A_C L^{\text{post}}$ of the post-combustion.

Four contributions might modify the rate of accumulation of a chemical species in this zone:

- The gas entering this zone from the disengagement

$$\rho_{\text{emul}} A_c \left(U\left(L^{\text{bed}}\right) + U_{mf}\right) y_k^{\text{dis}}$$

- The gas entering this zone from the secondary air supply: $\dot{m}^{\text{sec}}_{\text{air}} y_k^{\text{sec}}$
- The gas leaving the furnace: $\lfloor \rho_{\text{emul}} A_c (U(L^{\text{bed}}) + U_{\text{mf}}) + \dot{m}^{\text{sec}}_{\text{air}} \rfloor y_k^{\text{post}}$
- The net chemical reaction rate of that species: $A_c L^{\text{post}} R_k^{\text{post}}$

Given the rate of accumulation of that species in the control volume $A_c(\partial \rho_{\text{emul}} L^{\text{post}} y_k^{\text{post}}/\partial t)$ the following balance equation is derived

$$A_c \frac{\partial \rho_{\text{emul}} L^{\text{post}} y_k^{\text{post}}}{\partial t} = A_c \rho_{\text{emul}} \left(U\left(L^{\text{bed}}\right) + U_{mf}\right)\left[y_k^{dis} - y_k^{\text{post}}\right] + \dot{m}^{\text{sec}}_{\text{air}}\left[y_k^{\text{air}} - y_k^{\text{post}}\right] + A_c L^{\text{post}} R^{\text{post}}_{y_k}$$

The same formalism used in the case of total enthalpy would lead to an equivalent equation.

Chemical Reaction Rate. As in the case of the bubble zone, this region is expected to be free of solid. Thus, only volatile combustion and pollutant formation may affect chemical reaction rate within this region. As explained in the paragraph devoted to chemical reaction rate in the buffer zone, chemical equilibrium is supposed to be reached during volatile combustion. Their chemical reaction rates are evaluated through equilibrium tables. Dealing with pollutant formation, the assumption used in the buffer zone prevails.

Volumetric Heat Generation. Because of the choice of total enthalpy to represent the energetic level of the system, because of the lack of solid particles within this zone, and because impact of pollutant formation on energetic level is neglected, the volumetric heat generation is zero

$$R_H^{\text{post}} = 0$$

Manuscript received Jan. 10, 2000, and revision received Oct. 2, 2000.